



FACULTAD DE CIENCIAS
UNIVERSIDAD DE CANTABRIA

**Search for dark matter production in
association with top quarks in the
dilepton final state at $\sqrt{s} = 13$ TeV**

A thesis submitted in fulfillment of the requirements for the
Degree of Doctor of Philosophy

Written by
Cédric Prieëls

Under the supervision of
Jónatan Piedra Gómez
Pablo Martínez Ruiz del Árbol

Santander, June 2020



FACULTAD DE CIENCIAS
UNIVERSIDAD DE CANTABRIA

**Búsqueda de materia oscura en
asociación con quarks top en el estado
final dileptónico a $\sqrt{s} = 13$ TeV**

Memoria para optar al
Grado de doctor

Escrita por
Cédric Prieëls

Bajo la supervisión de
Jónatan Piedra Gómez
Pablo Martínez Ruiz del Árbol

Santander, Junio 2020

Abstract

Resumen

Acknowledgments

Acronyms used

ADMX	Axion Dark Matter Experiment	DY	Drell-Yan
ALICE	A Large Ion Collider Experiment	ECAL	Electromagnetic Calorimeter
AMS	Alpha Magnetic Spectrometer	EDM	Event Data Model
AOD	Analysis Object Data	EFT	Effective Field Theory
ATLAS	A Toroidal LHC ApparatuS	EWK	Electroweak
BDT	Boosted Decision Trees	FR	Fake Rate
BR	Branching Ratio	FSR	Final State Radiation
BSM	Beyond the Standard Model	GEM	Gas Electron Multiplier
BW	Breit-Wigner	GSF	Gaussian Sum Filter
CAST	CERN Axion Solar Telescope	HCAL	Hadronic Calorimeter
CERN	European Council for Nuclear Research	HLT	High-Level Trigger
CL	Confidence Level	HO	Hadron Outer
CMB	Cosmic Microwave Background	IACT	Imaging Atmospheric Cherenkov Telescopes
CMS	Compact Muon Solenoid	IAXO	International AXion Observatory
CSC	Cathode Strip Chamber	ISR	Initial State Radiation
CR	Control Region	KF	Kalman Filter
CSV	Combined Secondary Vertex	L1	Level-1 Trigger
CTA	Cherenkov Telescope Array	LAT	Fermi Large Telescope
DAQ	Data Acquisition System	LEP	Large Electron Positron collider
DAS	Data Aggregation System	LHC	Large Hadron Collider
DCS	Detector Control System	LNGS	Laboratori Nazionali del Gran Sasso
DQM	Data Quality Monitoring	LO	Leading Order
DM	Dark Matter	LS	Long Shutdown
DMWG	Dark Matter Working Group	MACHO	Massive Compact Halo Object
DNN	Deep Neural Network	MC	Monte Carlo
DT	Drift tube	MET	Missing Transverse Energy

MFV	Minimal Flavour Violation	RMS	Root Mean Square
ML	Machine Learning	RPC	Resistive Plate Chamber
MPI	Multiple Parton Interaction	SC	Super Cluster
MSSM	Minimal Supersymmetric Standard Model	SD	Spin Dependent
MVA	Multi-Variate Analysis	SF	Scale Factors
NFW	Navarro-Frenk-White	SI	Spin Independent
NLO	Next to Leading Order	SM	Standard Model
PDF	Parton Density Function	SPS	Super Proton Synchrotron
PF	Particle Flow	SR	Signal Region
POG	Physics Object Group	TEC	Tracker EndCap
PR	Prompt Rate	TIB/TBD	Tracker Inner Barrel and Disks
PS	Proton Synchrotron	TOB	Tracker Outer Barrel
PU	Pile Up	UE	Underlying Event
PUPPI	Pileup Per Particle Identification	UED	Universal Extra Dimensions
PV	Primary Vertex	VBF	Vector Boson Fusion
QCD	Quantum ChromoDynamics	WIMP	Weakly Interactive Massive Particle
QFT	Quantum Field Theory	WP	Working Point

Contents

1	Data, signals and backgrounds	1
1.1	The Monte Carlo (MC) simulation method	1
1.2	Files format	5
1.3	Analysis code	6
1.4	Data samples	6
1.5	Signal samples	6
1.6	Backgrounds prediction	6
1.6.1	Top production	7
1.6.2	Drell-Yan estimation	9
1.6.3	$t\bar{t} + V$	9
1.6.4	Non prompt contamination	10
1.6.5	Smaller backgrounds	15
1.6.6	Weights and corrections applied	15
2	Event selection	17
2.1	Objects selection	17
2.1.1	Triggers selection	17
2.1.2	Electrons selection	19
2.1.3	Muons selection	20
2.1.4	Jet selection	22
2.2	Signals regions	23
2.2.1	t/\bar{t} +DM region	24
2.2.2	$t\bar{t}$ +DM region	24
2.3	Control regions	25
2.3.1	Drell-Yan (DY) control region	25
2.3.2	Top control region	25
2.3.3	$t\bar{t}V$ control region	25
2.3.4	Same sign control region	25
2.4	Background-signal discrimination	27
2.4.1	Discriminating variables	27

2.4.2	Neural network	28
3	Results and interpretations	29
3.1	Systematics and uncertainties	29
3.2	Results	29
4	Conclusions	31
4.1	Future prospects	31
	Appendices	33
A	Samples used	35
A.1	Data samples	35
A.2	Signal samples	35
A.3	Backgrounds samples	35
B	Neural network optimization	43
	Bibliography	47

Chapter 1

Data, signals and backgrounds

In order to find a possible hint of the production of Dark Matter (DM) in the Large Hadron Collider (LHC) collisions considering our signal models of interest, briefly described in Section ??, the data collected needs to be compared with Monte Carlo (MC) simulations produced in a central way for each Standard Model (SM) process. Indeed, any deviation of the data observed with respect to what we expect to see, obtained from these MC simulations, might be the sign of some Beyond the Standard Model (BSM) physics. All of the steps needed to mathematically simulate the pp collisions of the LHC and to take into account the effect of the detector on the particles produced will first of all be introduced in Section 1.1.

Then, the different formats of files available to perform the analysis and the code used will be briefly introduced in Sections 1.2 and 1.3 and the different data samples collected during the Run II of operation of the LHC will be then detailed in Section 1.4, while the signal models and samples considered in this particular analysis along with the MC samples used for the simulation of the different backgrounds will be introduced in Sections 1.5 and 1.6 respectively.

1.1 The Monte Carlo (MC) simulation method

As previously explained, the generation of MC simulations for the most common SM processes is a crucial step of any analysis because they are considered to be the reference to which the data collected is compared in order to try and find some discrepancies, which could be the sign of the existence of BSM physics. Searches for exotic physics therefore heavily depend on these simulations, which need to be generated with great care and to which a large uncertainty is typically associated since the collision between the partons of two protons and the interaction between the particles produced and the detector itself are extremely complex by nature.

The basic idea of the MC simulation consists in using a random number generator to simulate the randomness of nature and produce as many events as computationally possible for all the SM processes, taking into account the probability density functions of these processes. This is performed by specific softwares called **event generators** and it is important to note that since we usually don't know everything about the SM or BSM process being generated, the perfect event generator does not exist.

To make the generation of such simulations a bit easier, the description of a typical pp collision can usually be divided into several steps that will now be described, as shown with the color code used in Figure 1.1. The typical approximations used to make this kind of simulation possible from the computational point of view will also be briefly introduced at this point.

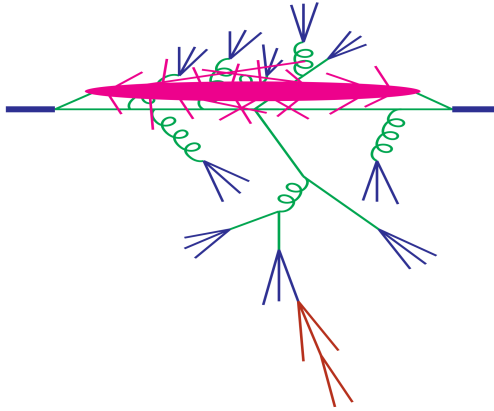


Figure 1.1: Structure of a pp collision and different steps of the MC simulation used by the event generators, such as the parton shower (in green), the Underlying Event (UE) (in pink), the hadronization (in blue) and the decay of unstable particles (in red) [101].

Hard scattering

A typical pp collision at a center of mass energy \sqrt{s} is usually described by an event generator as the interaction between a parton i coming from one proton with a parton j coming from the other, leading to the production of a final state A , made out of n different particles. The total cross section of such process can be expressed with Equation 1.1 [102].

$$\sigma_A(s) = \sum_{i,j} \iint dx_1 dx_2 f_i(x_1, \mu^2) f_j(x_2, \mu^2) \hat{\sigma}_{ij \rightarrow A}(\hat{s}, \mu^2) \quad (1.1)$$

In this equation, several variables have been introduced, such as:

- The artificial parameter μ^2 used as the delimitation between short and long range physics.
- The Parton Density Functions (PDFs) $f_i(x, \mu^2)$ of both partons involved in the collision, giving the probability of finding in the proton a parton of flavor i (quark or gluon) carrying a fraction x of the proton momentum.
- The integrated parton-level cross section $\hat{\sigma}_{ij \rightarrow A}$ describing the short range physics between the partons, taking into account the phase space and the matrix element obtained considering all the Feynman diagrams of a given process.
- The square invariant mass of the two partons $\hat{s} = (p_i + p_j)^2$.

Many algorithms have been developed in order to select a hard process $ij \rightarrow A$ and determine its kinematics by solving this equation using different methods. The samples used in this work have actually been produced at different orders and by different hard scattering generators, such as MADGRAPH [104] (at LO) and POWHEG [105] and MC@NLO [106] (at NLO).

Parton showers

The parton shower phase is then used to describe what happens to the incoming and outgoing partons after the initial collision that has just been described. The hard process induce by definition

a large acceleration to the partons involved, which then tend to emit Quantum ChromoDynamics (QCD) radiation under the forms of gluons, just like accelerated electric charges do by emitting photons. However, the gluons emitted do have a color charge and can therefore emit further radiation until reaching such a low energy that they are able to form colourless hadrons, as discussed in Section ???. This process typically leads to the creation of the so-called **parton showers**, approximate higher-order real-emission corrections to the hard scattering, that need to be simulated by the event generators as well since they are an important part of the kinematics of the collision.

The parton showering then consists in simulating these showers for not only the final state particles produced by the hard scattering, but also for the particles in the initial state and for the remnants of the colliding protons, since gluons can actually be emitted by Initial State Radiation (ISR) and by these remnants themselves.

Underlying Event (UE)

Once the hard scattering and all the possible gluon emissions simulated, the next step consists in considering the so-called **Underlying Event (UE)** arising from the parton showers just described and from the secondary collisions between partons not involved in the primary hard process, the so-called Multiple Parton Interactions (MPIs). The UE is usually responsible for the production of particles at low transverse momenta p_T that cannot be experimentally distinguished from particles produced from initial or final state radiation but still need to be simulated.

These secondary collisions typically lead to the production of extra hadrons and therefore need to be simulated as well by events generators, usually by distributing the partons of the incoming protons in an area of 1fm^2 : an increased UE will be obtained when the so-called impact parameter, the distance between the parton and the centre of this area, is decreased, making the collision mostly central and almost head-on [107]. The UE is typically well simulated using softwares such as Herwig [108] and PYTHIA [109]. The spectrum for the generation of some variables in a top enriched sample can be found in Figure 1.2.

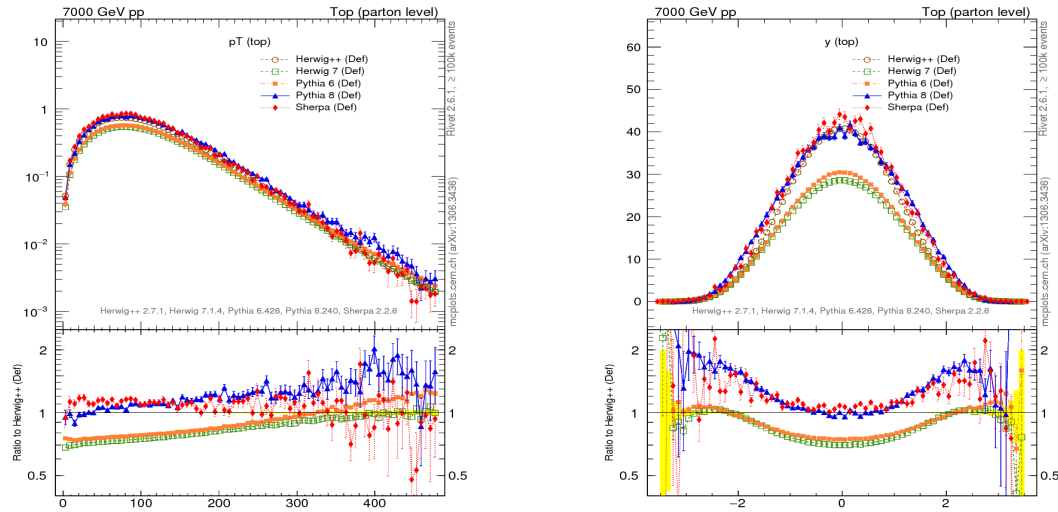


Figure 1.2: Top p_T (on the left) and rapidity (on the right) distributions obtained using different MC generators [110].

Hadronization

Once all the primary and secondary collisions simulated, it is time for the event generators to simulate the **hadronization** and binding processes of the different coloured partons emitted into colourless hadrons, as explained in Section ???. This hadronization process happen at low energies, when the perturbation theory becomes invalid and the dynamics enter a non-perturbative phase, which leads to the formation of the observed final-state hadrons. Non-perturbative calculations then have to be used by the event generators in order to simulate this effect.

Unstable particle decays

The last step of the MC generation consists in finding a model allowing the unstable hadrons created in the hadronization process to decay, and to study these decays. This is extremely important because experimental data clearly shows that a large fraction of the observed final state particles come from the decays of such excited hadronic states.

Detector simulation

Once the event completely simulated using the event generators and the Pile Up (PU) taken into account by reproducing the hard scattering process several times, another step is required: simulating the interaction between the "perfect" particles previously created and the "imperfect" Compact Muon Solenoid (CMS) detector.

This is typically done by the GEANT4 software [111], able to model different effects, such as:

- Modeling of the interaction region
- Modeling of the particle passage through the volumes that compose CMS detector and of the accompanying physics processes
- Modeling of the effect of multiple interactions per beam crossing and/or the effect of events overlay (PU simulation)
- Modeling of the detector's electronics response

This modeling accounts for all the cracks and for the disposition of the subsystems inside of the CMS detector. This software is for example able to model the interaction of the electrons with the tracker, responsible for the emission of bremsstrahlung photons, as explained in Section ??.

The results of the comparison between the output of two different versions of the GEANT4 software and prototypes of the CMS calorimeter in the test beam facility at European Council for Nuclear Research (CERN) lead to comparable results, as shown in Figure 1.3.

However, the modeling of the detector is not perfect and not all the inefficiencies can be accounted for. In some cases, Scale Factors (SF) are then used to correct the MC simulations and correct some expected discrepancies between data and MC. This will be detailed later on.

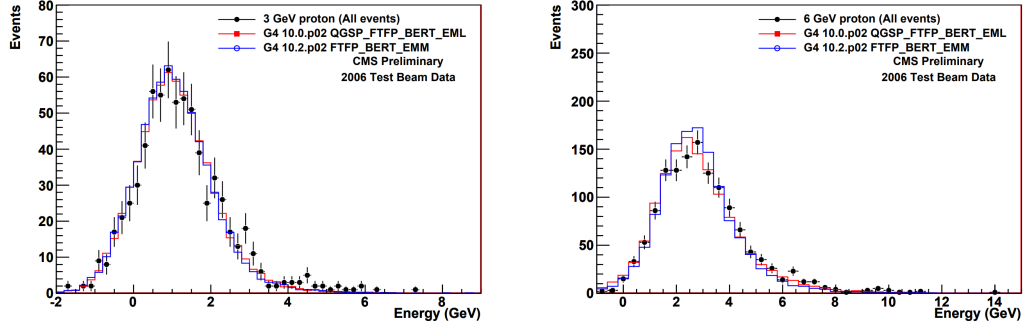


Figure 1.3: Proton energy distribution at 3 (on the left) and 6 (on the right) GeV compared for the test beam data (in black) and two different GEANT4 versions [112].

1.2 Files format

Once recorded (or simulated), the data (or MC) still needs to go under a complete post-processing in order to change its format and reduce the total size of the samples to be considered in the analyses. Different types of analysis are expected to need different levels of data reduction, so the data is usually accessible at different levels [113]:

- Virgin-RAW: used only in low rate runs with heavy ions collisions (10-15Mb/event)
- RAW : standard raw data event content (1Mb/event)
- RECO: detailed information on reconstructed physics objects (3Mb/event)
- Analysis Object Data (AOD): physics objects used in analysis (400-500kB/event)

Two additional formats were introduced since the end of the Run I. First of all the MiniAOD was introduced to reduce the size of the AOD by a factor 10 while retaining most of the information about all the particles that were created, without applying any further selection.

Because of the increased integrated luminosity collected by CMS over the last few years, a brand new file format featuring another reduction of the file size of a factor ~ 50 was recently introduced: the nanoAOD, able to retain most of the information of each collision in around 1kB of data per event only. This reduction in size was achieved by optimizing the floating point of the variables, by not storing quantities that can be recomputed from the available information and by limiting the number of physics objects available, for example. This means that some low-level analyses cannot use this format to work, but it has been estimated that around 50-70% of the analyses performed at CMS can rely on such files in order to work.

In this particular case, the 6th version of the nanoAOD, introducing a series of bug fixes and the latest jet energy corrections, was used for both the data and the MC samples (signal and backgrounds) that will now be listed in the next sections.

1.3 Analysis code

The code used for the event generation, simulation and reconstruction is the version 10.2.X of the official software of the CMS collaboration, called CMSSW [115]. This software contains the CMS Event Data Model (EDM) which is able to describe every event as a C++ object containing all the RAW and reconstructed information related to the collision. These objects are stored using the ROOT file format [116], an analysis package written in C++.

Once all the different samples produced centrally up to the nanoAOD stage, another framework was put in place in order to do a post-processing of such samples, by selecting objects interesting for different dileptonic analyses, reducing therefore even more the size of the samples to be considered by selecting only events having 2 tight leptons. This selection will be detailed in Chapter 2. This *Latino* framework, written in python, is common to several different analyses and has been developed by tens of different people over the past few years, providing several tools to produce samples, read the files, apply different corrections to the MC samples and produce the histograms needed to perform a search such as this one.

1.4 Data samples

As already explained in Section ??, the data analyzed in this work has been taken at a center of mass energy of 13 TeV during the second part of the Run II of operation of the LHC.

During this period, an integrated luminosity of $35.9 \pm 0.9 \text{ fb}^{-1}$ (2016) [117], $41.5 \pm 1.0 \text{ fb}^{-1}$ (2017) [118] and $59.7 \pm 1.5 \text{ fb}^{-1}$ (2018) [119] has been collected, resulting in a total dataset of $137.1 \pm 2.0 \text{ fb}^{-1}$ recorded by the CMS detector and ready to be analyzed. This data has been obtained by combining a set of single and double lepton triggers that will be described in Section 2.1.1 by taking care of avoiding any eventual double counting due to events present in different triggers. All the data samples considered for this analysis are listed in Section A.1.

1.5 Signal samples

To be completed once the files are actually available Listed in Section A.2.

1.6 Backgrounds prediction

Several different SM background processes have been considered for this analysis, all listed in Section A.3 and mostly estimated directly from MC. In this section, the main backgrounds to consider for this particular analysis will be reviewed, such as:

- The major background for the $t\bar{t}$ +DM analysis, the SM $t\bar{t}$, kinematically really close to the signal searched for (Section 1.6.1).
- On the other hand, the major background for the t/\bar{t} +DM analysis is the single top production, which has an even higher cross section than the $t\bar{t}$ (Section 1.6.1).

- Then, mainly because of its huge cross section at 13 TeV, as shown in Figure 1.4, the DY process is usually important to consider. Even though quite reduced in the Signal Regions (SRs) because of the cuts applied, a specific Control Region (CR) will be dedicated to check this background, taken directly from MC (Section 1.6.2).
- The $t\bar{t} + V$ ($t\bar{t} + Z$ and $t\bar{t} + W$) may have a kinematics even closer to our $t\bar{t}$ +DM signal than the $t\bar{t}$ process and is therefore extremely important in our signal regions, even though its low cross section does limit its impact (Section 1.6.3).
- Finally, the non-prompt background is another important piece of this analysis mainly because of the particular data-driven method used to compute them (Section 1.6.4).

Add percentage of each background once known

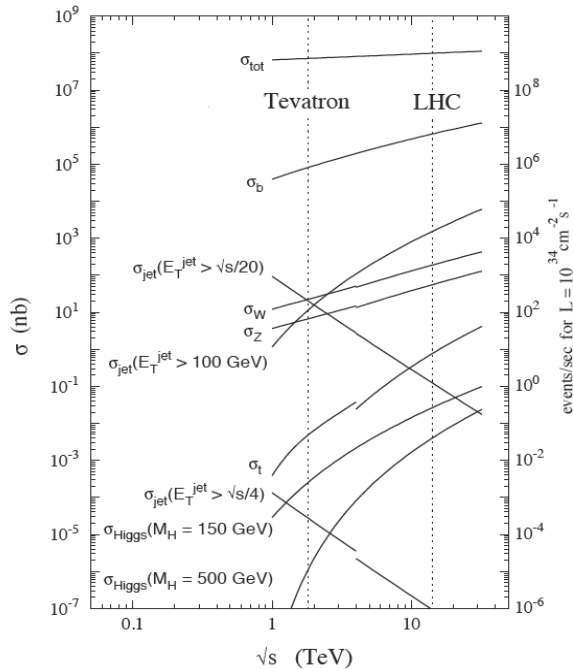


Figure 1.4: Production cross section of the most common SM processes considering different center of mass energies, such as the 13 TeV of the LHC.

Finally, some smaller backgrounds will be introduced in Section 1.6.5, such as the diboson and triboson production, and the weights and corrections applied to all these MC samples will be detailed in Section 1.6.6.

1.6.1 Top production

Because of the relatively high production cross section of top quarks at 13 TeV, the production of a single or a pair of top quarks, but without the production of associated DM, is obviously the dominant background in both searches.

They also have a kinematics quite close to the one expected for our signal: some additional Missing Transverse Energy (MET) is expected because of the production of a pair of DM particles, which might lead to a distribution ϕ distribution as well, but other than that achieving some

discrimination between these processes is quite complex. This process mostly relies on the use of Machine Learning (ML) techniques and will be fully detailed in Section 2.4.

Typically, given the importance of such processes, a specific CR to check for the validity of the CR of such processes is defined, as explained in Section 2.3.

The main background: $t\bar{t}$

Different Feynman diagrams contribute to this process at Leading Order (LO) in a hadron collider, as shown in Figure 1.5. This background is estimated directly from MC and, due to its importance, dedicated CRs have been designed in which to check for the data/MC agreement.

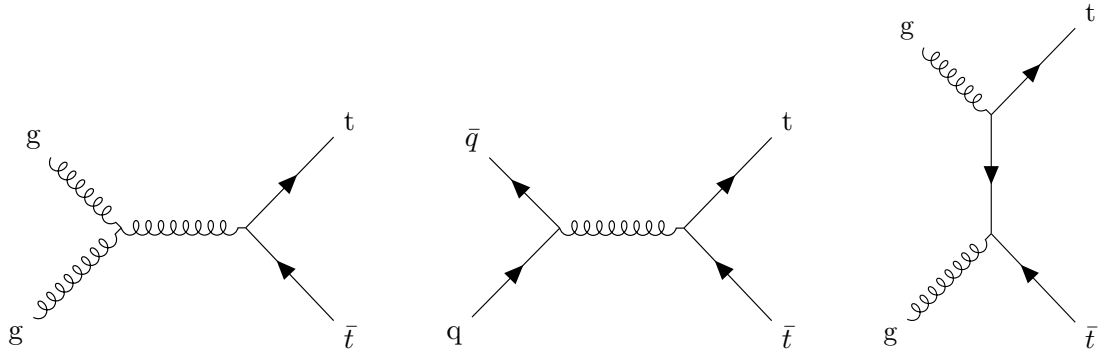


Figure 1.5: Main feynman diagrams for the production of the SM $t\bar{t}$ process.

Single top

Different Feynman diagrams also account for this process in the s-channel (Figure 1.6), t-channel and tW production mode (Figure 1.7).

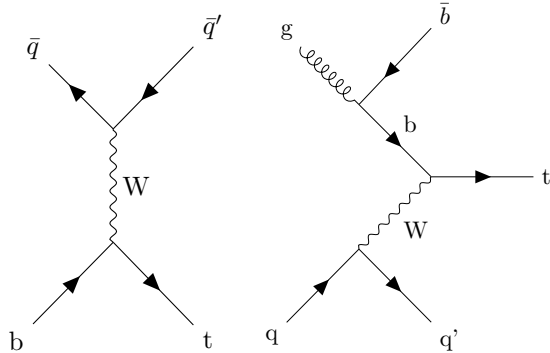


Figure 1.6: Feynman diagrams for s-channel production mode of a single top quarks.

Top decay

As previously mentioned, the top is the heaviest particle of the SM and is expected to decay inside of the beam pipe itself, usually into a bottom quark, giving us a b-jet, and a W boson; this boson can decay itself into different channels even though only its leptonic decay is consider in this particular case. The decay considered of the top/antitop produced is represented in Figure 1.8.

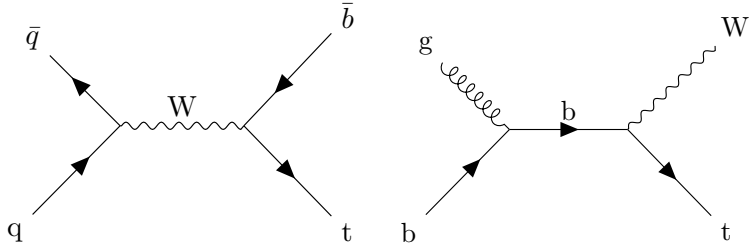


Figure 1.7: Feynman diagrams for t-channel (on the left) and tW (on the right) production modes of a single top quarks.

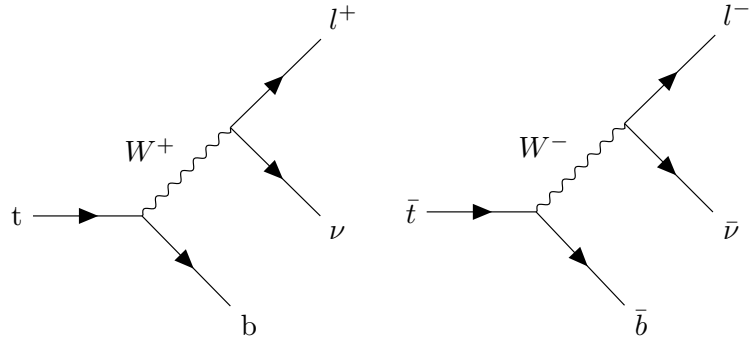


Figure 1.8: Feynman diagrams for the leptonic decay of the top (on the left) and antitop (on the right) quarks.

1.6.2 Drell-Yan estimation

As previously mentioned, most of the DY, produced through the Feynman diagram represented in Figure 1.9, is not expected to survive the selection applied to the analysis but because of the huge cross section of this process, two to three orders of magnitude larger than the production of top, the contribution of this process in the SRs is still quite important.

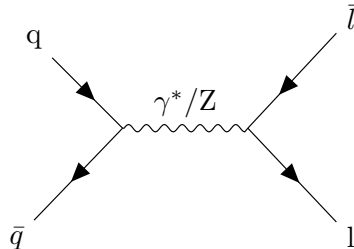


Figure 1.9: Feynman diagram for the DY process involving a virtual γ^* or Z boson.

This background is also estimated from MC as well and is being checked in a specific CR as well, as described in Section 2.3.

1.6.3 $t\bar{t} + V$

This background is coming from a usual $t\bar{t}$ production along with an ISR or Final State Radiation (FSR) production of a W or Z boson, as shown in Figure 1.10. The contribution of this background is also taken directly from MC.

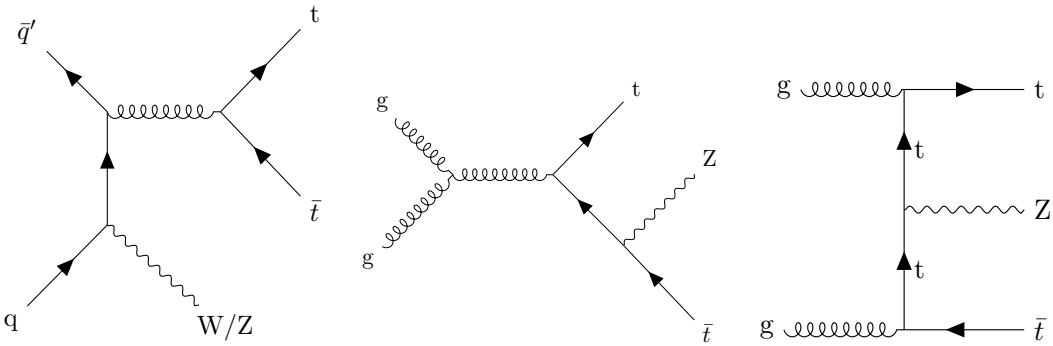


Figure 1.10: Possible Feynman diagrams for the Initial State Radiation (ISR) $t\bar{t}$ with a W/Z boson (on the left) and for the production of an Final State Radiation (FSR) ttZ (on the center and right).

The resulting cross section of such process is a bit lower than the production of the SM $t\bar{t}$ on its own but the kinematics of this background can be extremely close to our signal, since the W or Z boson produced can give a SM neutrino, leading to some actual MET.

1.6.4 Non prompt contamination

Even though not extremely important in the sense that its kinematics allow us to remove most of its contributions in the SRs, this background is interesting in the sense that it can be estimated using a data-driven method that will now be described instead of being taken directly from MC.

A few definitions are first of all needed to explain the method used to compute the importance of this background in the different regions of the analysis:

- First of all, a **prompt lepton** is defined as a real lepton, in the sense that the lepton is originating from the Primary Vertex (PV) of a pp collision.
- The **Prompt Rate (PR)** is defined as the number of prompt leptons passing the tight selection criteria of the analysis over the number of leptons passing the loose selection criteria.
- On the other hand, by **fake** or **non-prompt lepton**, we usually refer to truly **fake leptons**, such as jets misidentified by the detector as leptons, as shown in Figure 1.11, and real leptons coming from eventual heavy flavor decays.
- The **Fake Rate (FR)** is then defined similarly to the prompt rate but considering this time fake leptons only for the tight-to-loose ratio. This ratio therefore corresponds to the probability for a fake lepton to be considered as a real lepton in the analysis.

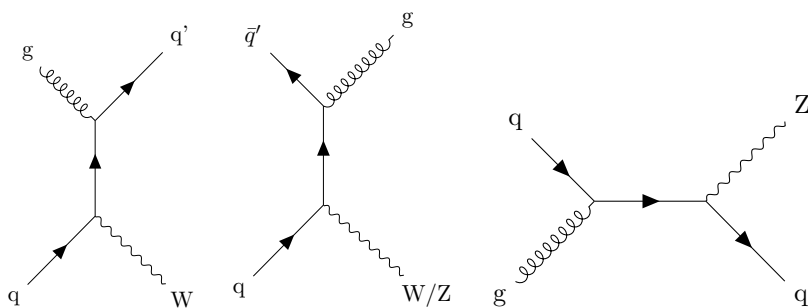


Figure 1.11: Possible Feynman diagrams for the production of a W/Z boson with a jet.

This background is particularly important at low p_T , where the misidentification rate is higher, and is not expected to be modeled correctly by MC because of its complexity: a general **tight-to-loose datadriven method** is then used to compute its kinematics and final contribution in the different regions of the analysis.

In general, this method contains three main steps: the computation of the FR and PR, the extension of these rates in a region kinematically close to the SR of the analysis and the definition of a same sign CR enriched in fakes in order to perform a closure test of the yields and kinematics of this background. All these steps will now be detailed.

Fake Rate (FR) computation

Because of its definition, the FR is computed in a prompt lepton-free region, typically in a loose QCD enriched region, defined with the following cuts:

- Exactly 1 lepton
- $mtw1 < 20$ GeV
- $p_T > 13$ (10) GeV for e (μ)
- PuppiMET < 20 GeV
- $|\eta| < 2.5$ (2.4) for e (μ)
- PassJets

All the previous cuts have been designed to define a loose QCD region as pure as possible by removing most of the W+jets and Z+jets contribution. The PassJets cut is a boolean obtained by looping over all the jets of the event trying to find a jet having an E_T higher than a given threshold in order to control the average p_T of the jet that fakes the lepton (actually, different FR have been computed for different E_T thresholds, from 10 to 50 GeV).

Using this method, the jet that fakes a lepton is actually the one recoiling against ($\Delta R > 1.0$) the jet used for the systematics, as shown in Figure 1.12.

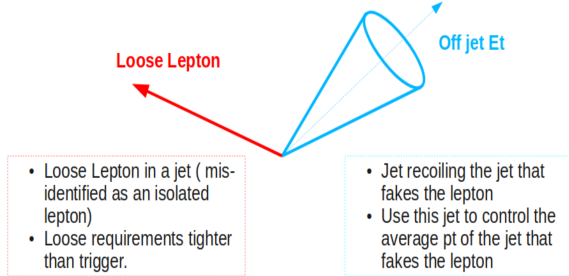


Figure 1.12: Schematic representation of the two jets used for the systematics and for the jet faking a lepton in the tight-to-loose datadriven method.

Events passing the following prescaled triggers are then selected in this region:

$$\text{Muon triggers} = \begin{cases} \text{HLT_Mu8_TrkIsoVVL (if } p_T < 20 \text{ GeV)} \\ \text{HLT_Mu17_TrkIsoVVL (if } p_T \geq 20 \text{ GeV)} \end{cases} \quad (1.2a)$$

$$\text{Electron triggers} = \begin{cases} \text{HLT_Ele8_CaloIdL_TrackIdL_IsoVL_PFJet30 (if } p_T < 25 \text{ GeV)} \\ \text{HLT_Ele23_CaloIdL_TrackIdL_IsoVL_PFJet30 (if } p_T \geq 25 \text{ GeV)} \end{cases} \quad (1.2b)$$

The remaining of the Electroweak (EWK) processes ($W+jets$, $Z+jets$) able to pass the previous cuts of the QCD region, are then simply subtracted: this is the so-called **EWK subtraction**.

Since both the FR and PR heavily depend on the kinematics of the event and on the Working Point (WP) chosen for the leptons of the analysis, they are computed separately depending on the flavor of the lepton and 2D histograms (accounting for the p_T and η of the event) need to be created at this stage to calculate this factor, for a given input jet E_T threshold; 1D histograms corresponding to the projections of these 2D histograms along both their axes are also defined at this point, as shown in Figure 1.13.

Prompt Rate (PR) computation

The PR, taking into account the real lepton contamination in the CR defined, is also important to calculate, even though the objects WP are usually chosen in such a way that this ratio is quite close to 1 and can therefore be ignored.

In our case, this rate has been calculated as well using a general tag and probe method in a $Z+jets$ enriched sample. The main objective is to reconstruct $Z \rightarrow ll$ events in this region and to select all the events for which the first lepton can be characterized as tight. Then, we search for the second lepton coming from the decay of Z within all the leptons detected by calculating the reconstructed mass of all the possible leptons combinations and selecting the one which is closer to the expected mass of the Z boson. We can then simply count how many times this second lepton, expected to be tight, has actually been measured as a tight lepton to estimate this PR.

The results obtained in this case have been represented in Figure 1.14

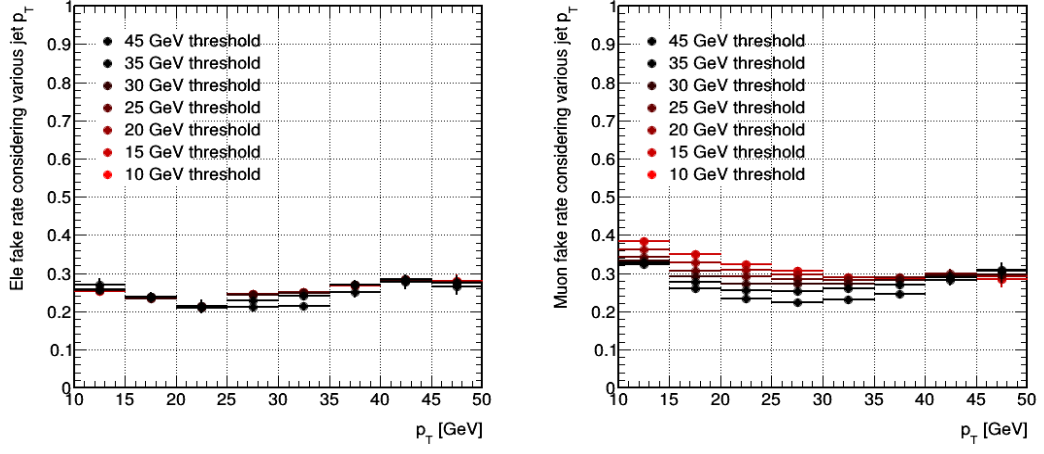
Fake weight calculation

Once the fake and prompt rates computed in their specific region, it is still necessary to apply them to a fake-lepton region kinematically close to the SRs of the analysis (usually, a l2loose region). For this, a simple set of equations can be used. We start by defining the following quantities:

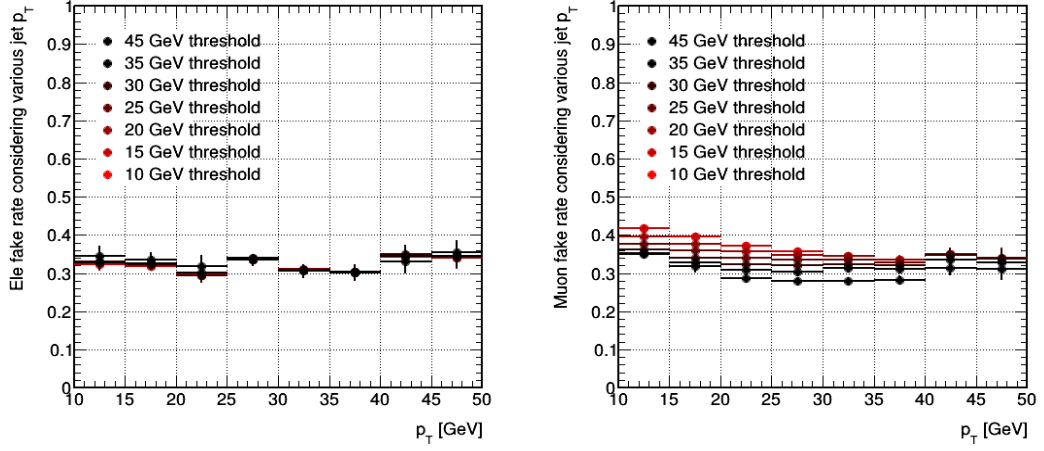
- N_{pp} events where both leptons are prompt
- N_{fp} events where one lepton is prompt and the other is fake
- N_{ff} events where both leptons are fake
- N_{tx} ($x = 0, 1, 2$) events with 0, 1 or 2 leptons passing the right cuts, the **only quantity directly measurable** by the detector

It is then possible to see in Equation 1.3 that, if p is the PR and f the FR previously calculated.

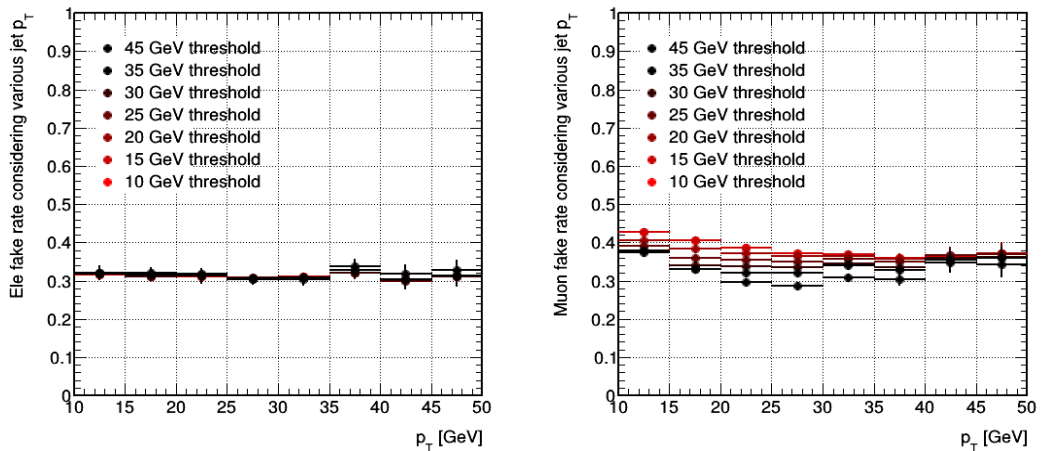
$$\left\{ \begin{array}{l} N_l = N_{pp} + N_{fp} + N_{ff} = N_{t2} + N_{t1} + N_{t0} \\ N_{t0} = (1-p)^2 N_{pp} + (1-p)(1-f)N_{fp} + (1-f)^2 N_{ff} \\ N_{t1} = 2p(1-p)N_{pp} + (f(1-p) + p(1-f))N_{fp} + 2f(1-f)^2 N_{ff} \\ N_{t2} = p^2 N_{pp} + pfN_{fp} + f^2 N_{ff} \end{array} \right. \quad (1.3)$$



(a) 2016 electron and muon fake rates

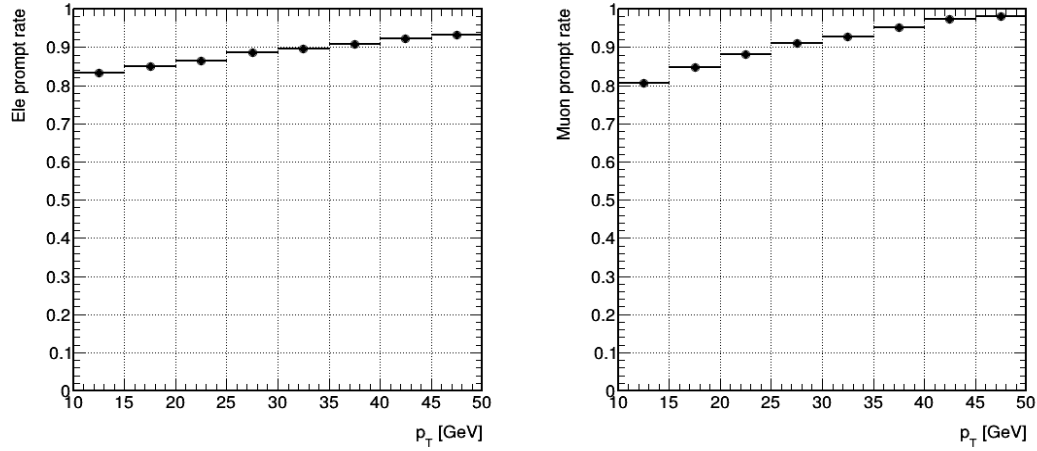


(b) 2017 electron and muon fake rates

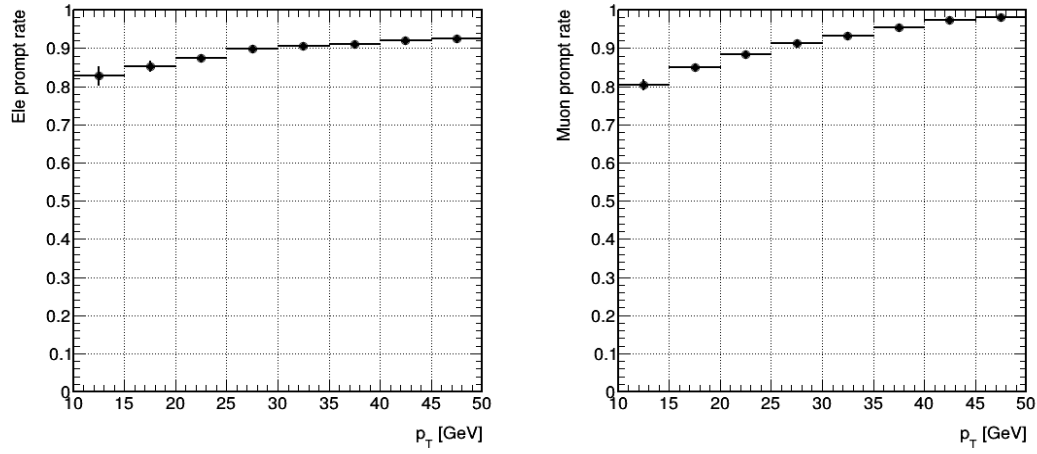


(c) 2018 electron and muon fake rates

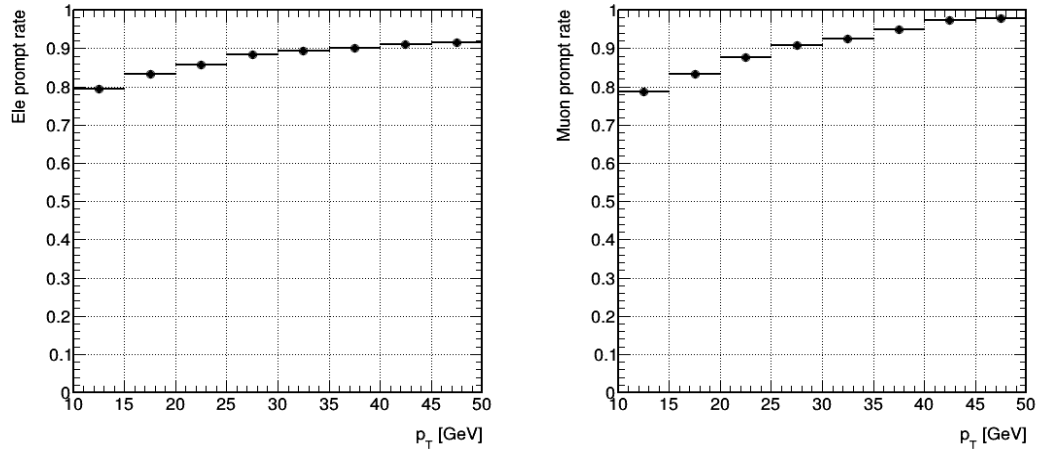
Figure 1.13: Electron (on the left) and muon (on the right) FR obtained in a QCD enriched region for different jet E_T thresholds for 2016, 2017 and 2018 with respect to the p_T of the lepton.



(a) 2016 electron and muon prompt rates



(b) 2017 electron and muon prompt rates



(c) 2018 electron and muon prompt rates

Figure 1.14: Electron (on the left) and muon (on the right) PR obtained in a $Z+jets$ enriched region by a general tag and probe method for 2016, 2017 and 2018 with respect to the p_T of the lepton.

These equations can be inverted in order to represent the unknowns with respect to the known variables, as shown in Equation 1.4, giving us a way to apply the weights previously calculated to this particular l2loose region.

$$\begin{pmatrix} N_{pp} \\ N_{fp} \\ N_{ff} \end{pmatrix} = \frac{f-p}{-(p-f)^3} \cdot \begin{pmatrix} f^2 & -f(1-f) & (1-f)^2 \\ -2fp & p(1-f) + f(1-p) & -2(1-p)(1-f) \\ p^2 & -p(1-p) & (1-p)^2 \end{pmatrix} \cdot \begin{pmatrix} N_{t0} \\ N_{t1} \\ N_{t2} \end{pmatrix} \quad (1.4)$$

Same sign control region

Now that we have a way to estimate the kinematics and yields of the non-prompt background in a different region, a same sign CR enriched in fakes is usually defined in order to check this background. This will be done and detailed in Section 2.3.4 of this work.

1.6.5 Smaller backgrounds

Even though quite negligible, some additional backgrounds still need to be considered, such as the dibosons (WW, WZ and ZZ) and tribosons (WWW, WWZ, WZZ, ZZZ) productions, as shown in Figure 1.15. Backgrounds such as the $W\gamma$ and Higgs related productions are also considered at this stage. All these smaller backgrounds are taken directly from MC.

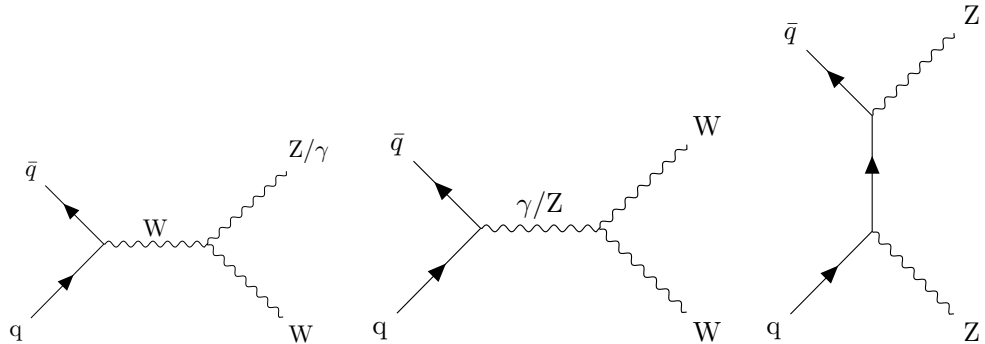


Figure 1.15: Possible Feynman diagrams for smaller backgrounds of this analysis: WW (on the left), $W\gamma$ and WZ (on the center) and ZZ (on the right).

1.6.6 Weights and corrections applied

Several different weights and Scale Factors (SF) usually need to be applied to the different MC processes in order to account for several effects observed in data but not accounted for during the generation of the MC simulation, such as the efficiency of the selection of the different objects, which will be discussed in Chapter 2, usually directly provided by the different Physics Object Groups (POGs) for their own default objects definitions.

In this section, several weights that are applied to the MC samples will be detailed.

Prefiring corrections

In 2016 and 2017 an issue, known as the **prefiring**, causing highly energetic readout from jets, photons and electrons in the Electromagnetic Calorimeter (ECAL) endcap to be assigned by the Level-1 Trigger (L1) to the previous bunch crossing was discovered. To make up for this difference, a weight $(1 - x)$ is usually applied to all MC events, where x is the probability of an event to be prefire [120].

The effect this correction has on the data/MC agreement in a 2017 top enriched control region is shown in Figure 1.16.

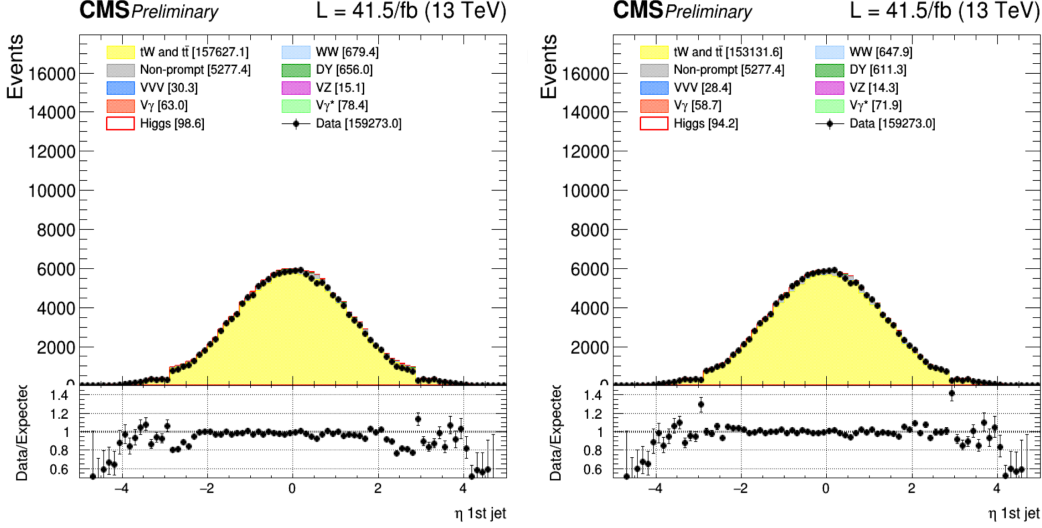


Figure 1.16: Data/MC agreement with (on the right) and without (on the left) prefiring corrections in a 2017 top control region.

Top p_T reweighting

Previous studies of the $t\bar{t}$ generator typically considered in the physics analysis predict a harder top quark p_T spectrum than the one observed in data [121].

Section to be completed with plots showing the effect of the weights

Chapter 2

Event selection

This Chapter will be dedicated to the analysis itself, by defining first of all the different objects actually used in this case, along with the actual selection that has been applied to enhance the quality of such objects in this particular search in Section 2.1. Then, the different Signal Regions (SRs) defined in which a high purity of signal is expected are defined in Section 2.2 while all the different Control Regions (CRs) defined in order to check the behavior of the MC simulation performed for the major backgrounds on this analysis, such as the single top or SM $t\bar{t}$ production, will be introduced in Section 2.3.

Finally will come a description about the different variables expected to naturally introduce some discrimination of the t/\bar{t} and $t\bar{t}+{\rm DM}$ signals with respect to the different backgrounds in Section 2.4, along with a global description of the Machine Learning (ML) techniques employed in order to optimize the discriminating power of these variables in the best way possible.

2.1 Objects selection

We already described what to expect from a typical t/\bar{t} or $t\bar{t}+{\rm DM}$ signal: the typical signature of such signals is made out of a certain number of b tagged jets along with two leptons (electrons and/or muons) and some Missing Transverse Energy (MET) coming from the two DM particles created along the way. It is therefore extremely important to describe the Working Point (WP) chosen and the selection applied in order to select the objects of the analysis, such as the leptons and the jets used, in such a way to optimize the lepton reconstruction efficiency while reducing as much as possible the possible misidentification rates of such objects.

First of all, the different triggers used to collect the data will be detailed in Section 2.1.1. Then, the leptons used in this analysis will be introduced in Sections 2.1.2 (for electrons) and 2.1.3 (for muons). Finally, given the nature of the DM signal searched for, a complete description of the jets selected in the analysis will be necessary and performed in Section 2.1.4.

2.1.1 Triggers selection

The triggers, described in Section ??, and particularly the trigger paths chosen are an important part of each analysis since they will describe the kind of data that can be collected and therefore analyzed. The triggers used in this analysis for the years 2016, 2017 and 2018 can be found in Tables 2.1, 2.2 and 2.1 respectively.

Dataset	Run range	High-Level Trigger (HLT) trigger path
SingleMu	[273158,284044]	HLT_IsoMu24_v* HLT_IsoTkMu24_v*
SingleEle	[273158,284044]	HLT_Ele27_WPTight_Gsf_v* HLT_Ele25_eta2p1_WPTight_Gsf_v*
DoubleEG	[273158,284044]	HLT_Ele23_Ele12_CaloIdL_TrackIdL_IsoVL_DZ_v*
DoubleMu	[273158,281612] [281613,284044]	HLT_Mu17_TrkIsoVVL_Mu8_TrkIsoVVL_v* HLT_Mu17_TrkIsoVVL_TkMu8_TrkIsoVVL_v* HLT_Mu17_TrkIsoVVL_Mu8_TrkIsoVVL_DZ_v* HLT_Mu17_TrkIsoVVL_TkMu8_TrkIsoVVL_DZ_v*
MuonEG	[273158,278272] [278273,284044]	HLT_Mu8_TrkIsoVVL_Ele23_CaloIdL_TrackIdL_IsoVL HLT_Mu23_TrkIsoVVL_Ele12_CaloIdL_TrackIdL_IsoVL HLT_Mu8_TrkIsoVVL_Ele23_CaloIdL_TrackIdL_IsoVL_DZ_v* HLT_Mu23_TrkIsoVVL_Ele12_CaloIdL_TrackIdL_IsoVL_DZ_v*

Table 2.1: 2016 trigger paths considered for this analysis.

Our analysis relying on the dilepton final state, the single lepton trigger are only considered in order to recover some of the efficiency lost in some cases when one lepton passes the tight identification criteria while the second one does not, and does therefore not trigger the event. The logical *or* of all the trigger paths are usually considered. Eventual events passing several triggers is taken into account as well to make sure to avoid any double counting due to this effect.

These triggers have been studied in order to make sure that they are efficient enough in the p_T region of the leptons of the analysis to avoid any undesired effect due to the turn-on of any trigger. These trigger efficiencies, calculated using a general tag and probe method and found for example for different runs of the 2017 data taking period in Figure 2.1 for a DoubleEG trigger, are then used to reweight the simulated samples.

Dataset	Run range	HLT trigger path
SingleMu	[297046,306462]	HLT_IsoMu27_v*
EGamma	[297046,306462]	HLT_Ele35_WPTight_Gsf_v* HLT_Ele23_Ele12_CaloIdL_TrackIdL_IsoVL_v*
DoubleMu	[297046,299329] [299368,306462]	HLT_Mu17_TrkIsoVVL_Mu8_TrkIsoVVL_DZ_v* HLT_Mu17_TrkIsoVVL_Mu8_TrkIsoVVL_DZ_Mass8_v*
MuonEG	[297046,306462] [297046,299329] [299368,306462]	HLT_Mu12_TrkIsoVVL_Ele23_CaloIdL_TrackIdL_IsoVL_DZ_v* HLT_Mu23_TrkIsoVVL_Ele12_CaloIdL_TrackIdL_IsoVL_DZ_v* HLT_Mu23_TrkIsoVVL_Ele12_CaloIdL_TrackIdL_IsoVL_DZ_v*

Table 2.2: 2017 trigger paths considered for this analysis.

Dataset	Run range	HLT trigger path
SingleMu	[315252,325172]	HLT_IsoMu24_v*
		HLT_Mu5_v*
	[314859,325175]	HLT_IsoMu27_v*
EGamma	[315252,325172]	HLT_Ele32_WPTight_Gsf_v*
		HLT_Ele35_WPTight_Gsf_v*
		HLT_Ele23_Ele12_CaloIdL_TrackIdL_IsoVL_v*
DoubleMu	[315252,325172]	HLT_Mu17_TrkIsoVVL_Mu8_TrkIsoVVL_DZ_Mass3p8_v*
		HLT_Mu17_TrkIsoVVL_Mu8_TrkIsoVVL_DZ_Mass8_v*
MuonEG	[315252,325172]	HLT_Mu23_TrkIsoVVL_Ele12_CaloIdL_TrackIdL_IsoVL_v*
		HLT_Mu12_TrkIsoVVL_Ele23_CaloIdL_TrackIdL_IsoVL_DZ_v*

Table 2.3: 2018 trigger paths considered for this analysis.

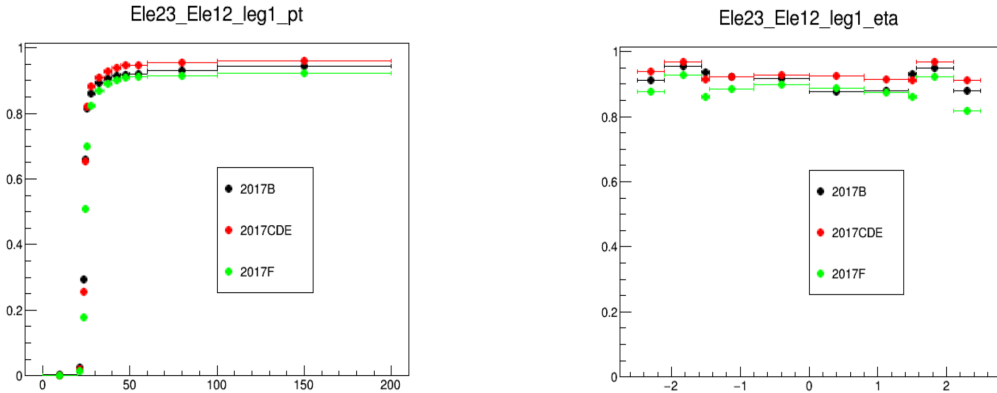


Figure 2.1: DoubleEG trigger efficiencies with respect to the p_T (on the left) and η (on the right), computed using a tag and probe method, for the 2017 data taking period.

2.1.2 Electrons selection

Several strategies are used in CMS in order to be able to identify prompt electrons and isolate this signal over background sources coming mainly from photon conversions, misidentification of jets or electrons coming from the semileptonic decay of the bottom and charm quarks. Several variables, which can be divided in the several following categories, allow to introduce some discrimination between these prompt and fake electrons:

- The **calorimetric observables** use the transverse shape of electromagnetic showers in the ECAL, the fact that these electromagnetic showers should be narrower than hadronic showers and the fraction of energy deposited in the Hadronic Calorimeter (HCAL) and in the preshower/endcaps of the ECAL itself for the discrimination. Many different variables belong to this category, such as:

- **hOverE** ($\frac{H}{E}$), where H corresponds to the energy deposited in the HCAL and E the total energy deposited in the ECAL.
- **ooEmooP** ($\frac{1}{E_{SC}} - \frac{1}{p}$), where E_{SC} is the Super Cluster (SC) energy and p the momentum of the track at the point of closest approach to the PV.

- **dEtaInSee** $\Delta\eta$ (**dPhiInSee** $\Delta\phi$), the η (ϕ) difference between the SC and the inner track extrapolated from the interaction vertex.
- **sigmaIetaIeta** ($\sigma_{\eta\eta}$), the weighted cluster Root Mean Square (RMS) inside 5x5 regions of SCs along η .
- The **isolation variables**, requiring the electron candidates to be quite isolated with respect to nearby energetic activity since most of the non-prompt electrons, such as electrons within a jet, are emitted with a large amount of surrounding energy.
 - The **relIsoWithEA** is the main variable that belongs to this category, corresponding to the Particle Flow (PF) isolation defined in a cone of size $\Delta R = 0.3$ around the electron direction and relative to the electron p_T , and taking into account the PU contamination in this cone.
- The **tracking quality variables**, such as:
 - The **expected inner hits**, the number of pixels without corresponding hits in the trajectory of a reconstructed gsfTrack.
 - The **matched gsfTracks hits**, the χ^2 value calculated from the reconstructed gskTrack and its corresponding hits.
- The **conversion rejection variables**, mostly used to reject most of the photon conversion contamination when defining electrons, using variable such as:
 - The **transverse d_0** (or d_{xy}) and **longitudinal d_z impact parameters**.
 - The **conversion veto**, checking if an electron candidate also matches at least one conversion candidate which also passes the selection cuts.

In this analysis, instead of relying on the four basic POG official Working Points (WPs) (veto, loose, medium and tight) that can be defined with some quality cuts, we rely on the Multi-Variate Analysis (MVA) approach that consists in using a single discriminator variable to perform the discrimination between genuine and misidentified electrons, combining the information coming from more than 20 variables at once using Boosted Decision Trees (BDT).

Two WPs are then given directly by the CMS EGamma POG [122], corresponding to an electron selection efficiency of 80 and 90% respectively. For this analysis, the tight POG *mva_90p_Iso2016* (for 2016) and *mvaFall17V1Iso_WP90* (for 2017 and 2018) WPs have been chosen for the electron definition, along with additional quality cuts defined in Tables 2.4 and 2.5 (as previously mentioned, these cuts sometimes differ quite a bit depending on whether the electron interacts with the ECAL barrel ($|\eta| < 1.479$) or one of the endcaps ($|\eta| \geq 1.479$)).

The electron efficiencies computed for this particular selection can be seen in Figure 2.2.

2.1.3 Muons selection

The selection applied to muons is mostly based on the Muon POG, providing references efficiencies for standard selection, recommendations for the tight selection [123], with a few additional cuts on both the impact parameters.

At the end of the day, a muon can be labeled as **Tight POG** if:

- The PF muon reconstructed is a global muon.

Variable		Barrel cut ($ \eta \leq 1.479$)	Endcap cut ($ \eta > 1.479$)
Basic selection			
$ \eta $	<	-	2.5
HLT safe selection			
hOverE	<	0.060	0.065
ooEmooP	<	0.013	0.013
$ \text{dEtaInSee}(\Delta\eta) $	<	0.004	-
$ \text{dPhiInSee}(\Delta\phi) $	<	0.020	-
$\sigma_{\eta\eta}$	<	0.011	0.031
ecalPFClusterIso	<	0.160	0.120
hcalPFClusterISO	<	0.120	0.120
trackIso	<	0.08	0.08
GsfTrack χ^2/NDOF	<	-	3.0
Additional selection			
lostHits	<	1	1
d_{xy}	<	0.05	0.1
d_z	<	0.1	0.2
pfRelIso03	<	0.0588	0.0571

Table 2.4: Quality cuts applied to define a 2016 tight electron in this analysis.

- The χ^2/NDOF of the global muon track fit is less than 10 and at least one muon chamber hit is included in the global muon track fit
- Muon segments in at least two muon stations have been observed.
- Its tracker track has a transverse impact parameter $d_{xy} < 0.2$ cm and a longitudinal impact parameter $d_z < 0.5$ cm with respect to the PV .
- The number of pixel hits is larger than 0.
- At least 5 tracker layers with hits have been observed.

The selection applied to muons of this particular analysis is a bit tighter though, since the following cuts are applied on top of this selection:

- $p_T > 10$ GeV, $|\eta| < 2.4$ and $|d_z| < 0.1$ cm
- $|d_{xy}| < 0.01$ cm (if $p_T < 20$ GeV) or $|d_{xy}| < 0.02$ cm (if $p_T \geq 20$ GeV)
- Tight muon isolation requirement (< 0.15) with $\Delta\beta$ correction and in a cone size $\Delta R < 0.4$, as defined in Equation 2.1, in order to reduce the number of muons coming from the hadronization process of bottom and charm quarks.

$$\text{ISO} = \frac{\sum p_T^{\text{ch. had. (PV)}} + \max(0, \sum E_T^{\text{neut. had.}} + \sum E_T^\gamma - 0.5 \times \sum p_T^{\text{ch. had. (PU)}})}{p_T(\mu)} \quad (2.1)$$

Variable		Barrel cut ($ \eta \leq 1.479$)	Endcap cut ($ \eta > 1.479$)
Basic selection			
$ \eta $	<	-	2.5
convVeto	=	1	1
d_{xy}	<	0.05	0.1
d_z	<	0.1	0.2
pfRelIso03	<	0.06	0.06

Table 2.5: Quality cuts applied to define a 2017/2018 tight electron in this analysis.

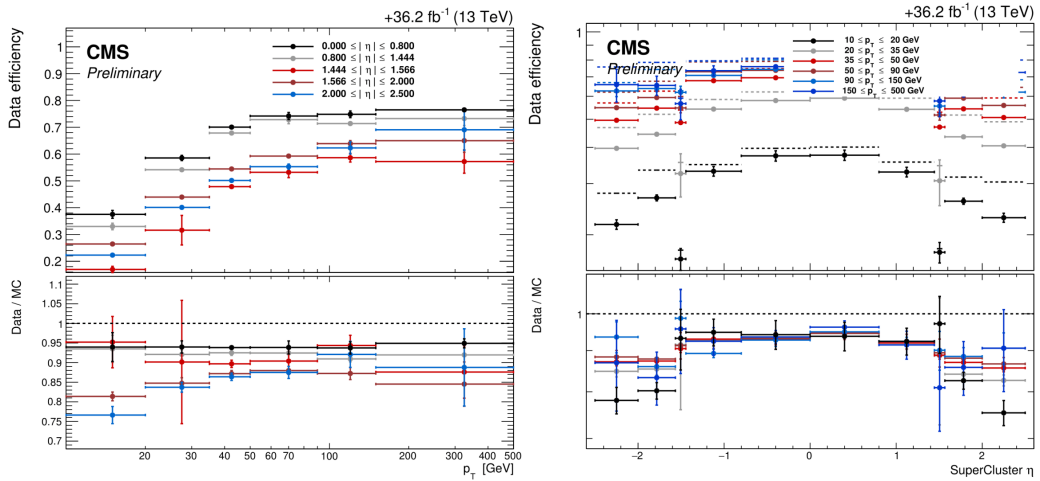


Figure 2.2: Tight electron efficiencies for this analysis, based on the Egamma POG `mva_90p_Iso2016` WP, for the data taking period of 2016.

This selection leads to efficiencies higher than 80% for all the muon momenta and pseudorapidities range, as shown in Figure 2.3.

2.1.4 Jet selection

Jets are an important part of this analysis as well given the final state searched for in this case. As explained in Section ??, the jets are clustered from the PF candidates using the anti-kT algorithm (with a typical distance parameter $R = 0.4$).

A selection is then applied on these jets in order to separate noise from real jets. In this analysis, this selection follows the tight WP definition given by the CMS JET/MET POG [124], whose selection depends on the pseudorapidity of the jet and on the year of data taking, as shown in Tables 2.6 and 2.7. The tight WP has been chosen since it offers an efficiency higher than 98-99% for all the jets and a background rejection higher than 98% for jets having $|\eta| < 3.0$.

A slightly different selection (loose PU jet ID) is applied to jets having a $p_T > 50$ GeV in order to reject jets coming from PU interactions in 2017 and 2018, as shown in Table 2.8.

The b-jets are then also select using the recommendations given by the B-Tagging and Vertexing POG [125]. The loose deepCSV b-tagging WP is used in this case, as explained in Section ??, for which the rate for misidentifying a light jet as a b-jet is around 10%. A jet is considered a b-jet in

p_T/η	-2.4:-2.1	-2.1:-1.6	-1.6:-1.2	-1.2:-0.8	-0.8:-0.3	-0.3:-0.2	-0.2:0.0	0.0:0.2	0.2:0.3	0.3:0.8	0.8:1.2	1.2:1.6	1.6:2.1	2.1:2.4
10:15	0.9995	1.0016	0.9985	0.9907	0.9844	1.0183	1.0089	1.0089	1.0265	0.9862	0.9808	0.9882	0.9927	0.9972
15:20	0.9805	0.9870	0.9950	0.9867	0.9935	0.9686	0.9927	0.9927	0.9771	0.9924	0.9826	0.9986	0.9912	0.9797
20:25	0.9756	0.9829	0.9949	0.9823	0.9914	0.9712	0.9906	0.9910	0.9590	0.9917	0.9776	0.9927	0.9873	0.9822
25:30	0.9793	0.9850	0.9942	0.9794	0.9912	0.9659	0.9899	0.9886	0.9610	0.9899	0.9784	0.9932	0.9874	0.9805
30:40	0.9773	0.9828	0.9947	0.9782	0.9891	0.9685	0.9903	0.9883	0.9614	0.9887	0.9770	0.9940	0.9876	0.9828
40:60	0.9766	0.9851	0.9957	0.9796	0.9908	0.9713	0.9911	0.9894	0.9638	0.9898	0.9786	0.9945	0.9871	0.9774
60:100	0.9618	0.9794	0.9963	0.9773	0.9917	0.9597	0.9914	0.9886	0.9655	0.9883	0.9764	0.9948	0.9858	0.9796
100:200	0.9803	0.9743	0.9831	0.9740	0.9949	0.9634	0.9954	0.9814	0.9482	0.9870	0.9732	0.9962	0.9782	0.9895

Color Definition

Scale Factors	0.99-1.01	0.98-0.99,1.01-1.02	0.97-0.98,1.02-1.03	0.96-0.97	0.95-0.96	< 0.95
---------------	-----------	---------------------	---------------------	-----------	-----------	--------

(a) 2016 muon efficiencies

p_T/η	-2.4:-2.1	-2.1:-1.6	-1.6:-1.2	-1.2:-0.8	-0.8:-0.3	-0.3:-0.2	-0.2:0.0	0.0:0.2	0.2:0.3	0.3:0.8	0.8:1.2	1.2:1.6	1.6:2.1	2.1:2.4
10:15	0.9880	0.9827	0.9981	0.9961	1.0018	1.0099	1.0129	1.0129	1.0193	0.9893	0.9767	0.9978	0.9901	0.9852
15:20	0.9735	0.9831	0.9955	0.9849	0.9995	0.9582	0.9932	0.9932	0.9400	0.9891	0.9813	0.9970	0.9899	0.9807
20:25	0.9737	0.9839	0.9976	0.9863	0.9940	0.9561	0.9936	0.9963	0.9757	0.9915	0.9800	0.9975	0.9892	0.9771
25:30	0.9741	0.9819	0.9975	0.9852	0.9931	0.9580	0.9936	0.9952	0.9619	0.9914	0.9790	0.9979	0.9905	0.9826
30:40	0.9719	0.9794	0.9973	0.9842	0.9935	0.9570	0.9932	0.9942	0.9635	0.9921	0.9781	0.9972	0.9900	0.9815
40:60	0.9709	0.9815	0.9979	0.9849	0.9941	0.9556	0.9945	0.9953	0.9636	0.9924	0.9790	0.9966	0.9896	0.9800
60:100	0.9622	0.9779	0.9959	0.9842	0.9935	0.9525	0.9938	0.9944	0.9563	0.9918	0.9747	0.9967	0.9868	0.9887
100:200	0.9649	0.9732	0.9899	0.9851	0.9884	0.9645	1.0060	0.9953	0.9831	0.9872	0.9738	0.9981	0.9868	0.9635

Color Definition

Scale Factors	0.99-1.01	0.98-0.99	0.97-0.98	0.96-0.97	0.95-0.96	< 0.95
---------------	-----------	-----------	-----------	-----------	-----------	--------

(b) 2017 muon efficiencies

p_T/η	-2.4:-2.1	-2.1:-1.6	-1.6:-1.2	-1.2:-0.8	-0.8:-0.3	-0.3:-0.2	-0.2:0.0	0.0:0.2	0.2:0.3	0.3:0.8	0.8:1.2	1.2:1.6	1.6:2.1	2.1:2.4
10:15	0.9686	0.9806	0.9996	0.9801	0.9975	0.9895	1.0053	1.0053	0.9446	0.9908	0.9763	0.9984	0.9967	0.9726
15:20	0.9683	0.9817	0.9974	0.9836	0.9951	0.9513	0.9925	0.9925	0.9678	0.9901	0.9849	0.9945	0.9888	0.9810
20:25	0.9681	0.9826	0.9979	0.9874	0.9963	0.9670	0.9936	0.9986	0.9725	0.9921	0.9835	0.9967	0.9899	0.9786
25:30	0.9679	0.9821	0.9977	0.9858	0.9960	0.9779	0.9943	0.9918	0.9795	0.9941	0.9804	0.9964	0.9890	0.9742
30:40	0.9688	0.9789	0.9970	0.9848	0.9956	0.9778	0.9933	0.9946	0.9740	0.9930	0.9814	0.9957	0.9885	0.9749
40:60	0.9672	0.9802	0.9967	0.9856	0.9964	0.9752	0.9950	0.9952	0.9743	0.9943	0.9821	0.9958	0.9875	0.9761
60:100	0.9652	0.9756	0.9959	0.9835	0.9957	0.9725	0.9919	0.9946	0.9760	0.9931	0.9803	0.9945	0.9853	0.9702
100:200	0.9500	0.9750	0.9944	0.9839	0.9976	0.9688	0.9984	0.9890	0.9460	0.9925	0.9778	0.9954	0.9780	0.9881

Color Definition

Scale Factors	0.99-1.01	0.98-0.99	0.97-0.98	0.96-0.97	0.95-0.96	< 0.95
---------------	-----------	-----------	-----------	-----------	-----------	--------

(c) 2018 muon efficiencies

Figure 2.3: Tight muon efficiencies for this analysis, based on the Muon POG tight WP with additional cuts for 2016, 2017 and 2018.

this analysis if it passes the following cuts:

- $p_T > 20 \text{ GeV}$
- $|\eta| < 2.4$
- $\text{deepCSV} > 0.1241$

2.2 Signals regions

It is important to note that a strict **blinding policy** has been followed for this search, in order to avoid optimizing the analysis based on what has already seen. The data available to be plotted in the following signal regions has therefore been limited to 1 fb^{-1} for each year.

Two signal regions have been defined in order to isolate on one hand the $t/\bar{t}+\text{DM}$ process and on the other hand the $t\bar{t}+\text{DM}$ signal.

Variable	$ \eta \leq 2.4$	$ \eta \leq 2.7$	$2.7 < \eta \leq 3.0$	$ \eta > 3.0$
Neutral Hadron Fraction	< 0.90	< 0.90	< 0.98	-
Neutral EM Fraction	< 0.99	< 0.99	> 0.01	< 0.90
Number of Constituents	> 1	> 1	-	-
Charged Hadron Fraction	> 0	-	-	-
Charged Multiplicity	> 0	-	-	-
Charged EM Fraction	< 0.99	-	-	-
Number of Neutral Particles	-	-	> 2	> 10

Table 2.6: JET/MET POG tight WP for 2016.

Variable	$ \eta \leq 2.4$	$ \eta \leq 2.7$	$2.7 < \eta \leq 3.0$	$ \eta > 3.0$
Neutral Hadron Fraction	< 0.90	< 0.90	-	> 0.02
Neutral EM Fraction	< 0.90	< 0.90	> 0.02 and < 0.99	< 0.90
Number of Constituents	> 1	> 1	-	-
Charged Hadron Fraction	> 0	-	-	-
Charged Multiplicity	> 0	> 0	-	-
Number of Neutral Particles	-	-	> 2	> 10

Table 2.7: JET/MET POG tight WP for 2017 and 2018.

2.2.1 t/\bar{t} +DM region

To be added once defined

2.2.2 $t\bar{t}$ +DM region

To be added once defined

Variable	$ \eta \leq 2.4$	$ \eta \leq 2.7$	$2.7 < \eta \leq 3.0$	$ \eta > 3.0$
Neutral Hadron Fraction	< 0.90	< 0.90	< 0.99	> 0.02
Neutral EM Fraction	< 0.90	< 0.90	-	< 0.90
Number of Constituents	> 1	> 1	-	-
Charged Hadron Fraction	> 0	-	-	-
Charged Multiplicity	> 0	-	-	-
Number of Neutral Particles	-	-	-	> 2 and < 15

Table 2.8: JET/MET POG tight WP for 2017 and 2018, for jets having a $p_T > 50$ GeV.

2.3 Control regions

Different control regions where the data/MC agreement can be checked have been defined in order to check the validity of the MC simulations performed for the SM processes corresponding to the main backgrounds of this analysis.

In this context, the DY control region will be defined in Section 2.3.1 while the SM $t\bar{t}$, WW and ttV processes will be checked in the Sections 2.3.2, ?? and 2.3.3 respectively.

2.3.1 DY control region

To be added once defined

2.3.2 Top control region

To be added once defined

2.3.3 ttV control region

To be added once defined

2.3.4 Same sign control region

A same sign control region has also been defined in order to check the non-prompt background, calculated using a data-driven tight-to-loose method described in Section 1.6.4. This CR is defined with the following cuts:

- Exactly 2 same sign leptons
- $p_{T,1} > 20$ (25) GeV for e (μ)
- $p_{T,2} > 13$ GeV
- $|\eta| < 2.5$ for both leptons
- $m_{ll} > 12$ GeV
- PuppiMET > 20 GeV
- $p_T^{ll} > 30$ GeV
- $m_{th} > 60$ GeV

Several regions are then defined according to this cut, depending on the data taking period, on the channel, on the number of jets observed and on the p_T of the second lepton. Some plots can be found in Figure 2.4.

In order to cover for most of the discrepancies between the data and the simulation observed in the distributions of this control region, a flat 30% systematic uncertainty is typically associated to this background, as will be discussed in more details in Section 3.1.

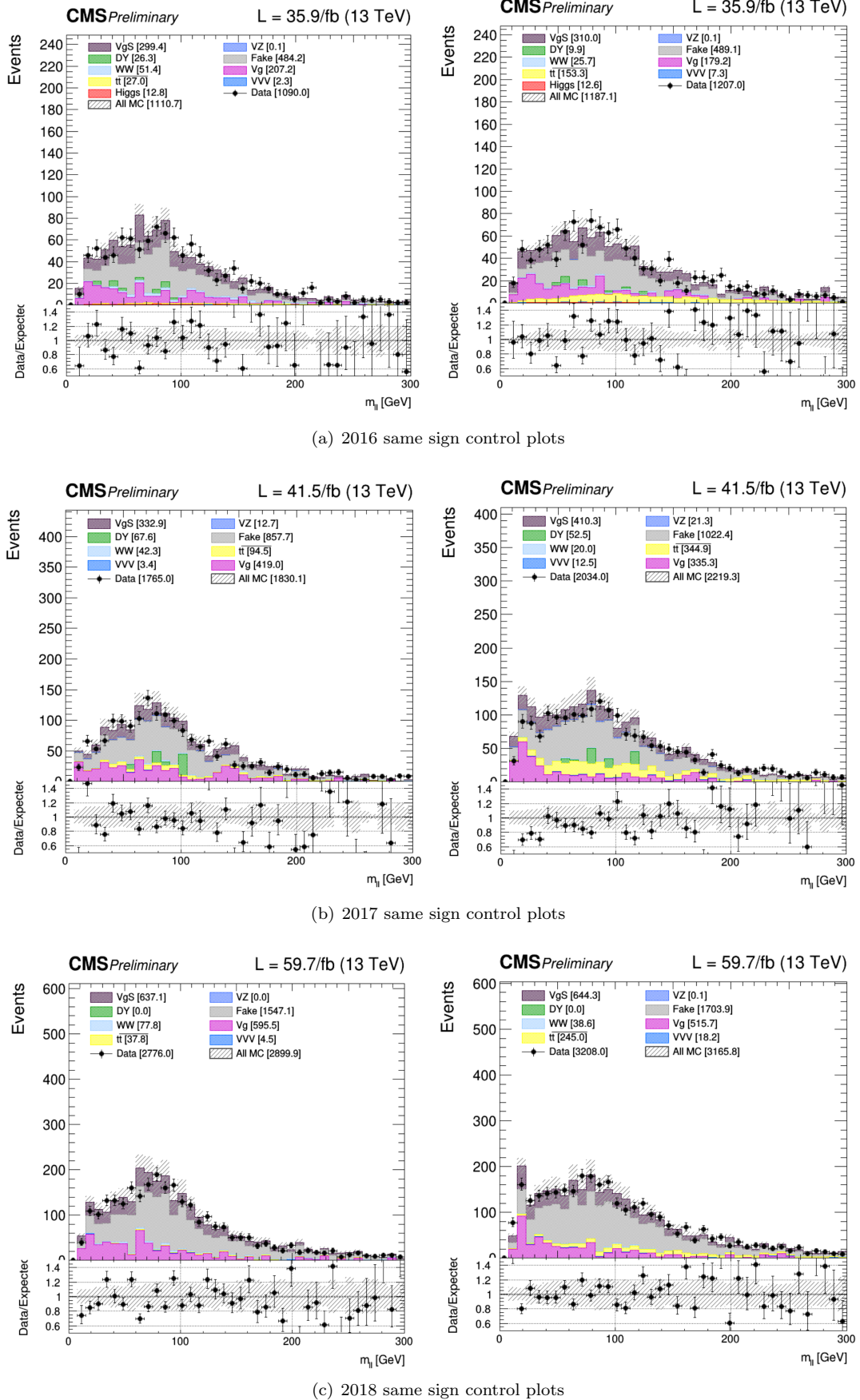


Figure 2.4: Same sign control region m_{ll} distributions for the years 2016, 2017 and 2018 and for the $e\mu$ channel and for the 0-jet (on the left) and 1j (on the right) categories.

2.4 Background-signal discrimination

2.4.1 Discriminating variables

Missing Transverse Energy (MET)

This variable has already been defined in Section ??, and corresponds to the imbalance in transverse momentum which can be left by different phenomena, such as the apparition of a SM neutrino or the existence of DM particles, able to escape the detector without being detected.

This variable is expected to induce some discrimination between the signal and the backgrounds because, even tough the $t\bar{t}$ in the dilepton final state is expected to produce two neutrinos and therefore some MET, the $t\bar{t}+DM$ signal model is expected to have mostly the same contribution to the MET from its own two neutrinos, and an additional contributions from the pair $\chi\bar{\chi}$ produced. The MET spectrum is therefore expected to reach higher values for the signal than the backgrounds.

TALK ABOUT SINGLE TOP?

Stransverse mass

The m_{T2} variable, also called **stransverse mass**, is an extension of the definition of the transverse mass m_T to cases when pairs of particles with the same flavor decay into one visible and one invisible particle, such as what happens in the $W \rightarrow l\nu$ decay, for example.

In this particular case, two particles contribute to the presence of Missing Transverse Energy (MET) and the individual contribution of each particle (\not{p}_{T_1} and \not{p}_{T_2}) to this missing energy cannot be inferred. The stransverse mass is then defined according to Equation 2.2, where $\not{p}_{T_i} = \vec{p}_T^i$ is the (visible) transverse momentum of the particle i and α is the angle between the visible and invisible p_T of the decay considered [114].

$$\begin{cases} M_{T2}^2 = \min_{\not{p}_{T_1} + \not{p}_{T_2} = \not{p}_{T_{\text{tot}}}} \left(\max \left(m_T^2(\not{p}_{T_1}, \not{p}_{T_1}), m_T^2(\not{p}_{T_2}, \not{p}_{T_2}) \right) \right) \\ m_T^2(\not{p}_T, \not{p}_T) = 4 |\not{p}_T| |\not{p}_T| \sin^2 \left(\frac{\alpha}{2} \right) \end{cases} \quad (2.2)$$

This equation can be understood in the following way: to compute the m_{T2} variable, different combinations $(\not{p}_{T_1}, \not{p}_{T_2})$ satisfying the condition $\not{p}_{T_1} + \not{p}_{T_2} = \not{p}_{T_{\text{tot}}}$ need to be probed, keeping only the combination which results in the lowest value.

In this particular analysis, $M_{T2}(ll)$ is calculated, since the role of the visible particles is played by the two final state leptons. This variable is expected to introduce some discrimination because, according to the definition just given, the $M_{T2}(ll)$ variable for a SM $t\bar{t}$ process is expected to have an endpoint exactly at the mass of the W boson, while an eventual $t\bar{t}+DM$ signal does not have this limitation in the $M_{T2}(ll)$ spectrum because of the pair of DM particles produced, which also contributes to the total MET of the event.

However, in practice, we do observe a tail in this spectrum even for SM $t\bar{t}$ without DM, because of the instrumental MET sometimes observed or the fact that some selected leptons are not actually

prompt leptons but can be jets misidentified as leptons by the detector.

TALK ABOUT SINGLE TOP?

2.4.2 Neural network

Chapter 3

Results and interpretations

3.1 Systematics and uncertainties

3.2 Results

Chapter 4

Conclusions

4.1 Future prospects

Appendices

Appendix A

Samples used

A.1 Data samples

All the data samples considered for this analysis are listed in Tables A.1, A.2 and A.3. The luminosity of each dataset has been computed using the Brilcalc tool provided by CMS [126], while the number of generated events has been obtained using the CERN official Data Aggregation System (DAS).

A.2 Signal samples

To be completed once the files are actually available

A.3 Backgrounds samples

All the background MC samples considered for this analysis are listed in Tables A.4, A.5 and A.6 for 2016, 2017 and 2018 respectively.

Dataset	Events (size)	\mathcal{L} [fb $^{-1}$]
Run 2016B		
/DoubleEG/Run2016B_ver2-Nano1June2019_ver2-v1/NANOAOD	143073268 (99.4Gb)	
/DoubleMuon/Run2016B_ver2-Nano1June2019_ver2-v1/NANOAOD	82535526 (53.2Gb)	
/MuonEG/Run2016B_ver2-Nano1June2019_ver2-v1/NANOAOD	32727796 (26.8Gb)	5.8
/SingleElectron/Run2016B_ver2-Nano1June2019_ver2-v1/NANOAOD	246440440 (167.8Gb)	
/SingleMuon/Run2016B_ver2-Nano1June2019_ver2-v1/NANOAOD	158145722 (96.4Gb)	
Run 2016C		
/DoubleEG/Run2016C-Nano1June2019-v1/NANOAOD	47677856 (35.3Gb)	
/DoubleMuon/Run2016C-Nano1June2019-v1/NANOAOD	27934629 (19.7Gb)	
/MuonEG/Run2016C-Nano1June2019-v1/NANOAOD	15405678 (12.8Gb)	2.6
/SingleElectron/Run2016C-Nano1June2019-v1/NANOAOD	97259854 (69.3Gb)	
/SingleMuon/Run2016C-Nano1June2019-v1/NANOAOD	67441308 (42.4Gb)	
Run 2016D		
/DoubleEG/Run2016D-Nano1June2019-v1/NANOAOD	53324960 (39.6Gb)	
/DoubleMuon/Run2016D-Nano1June2019-v1/NANOAOD	33861745 (24.1Gb)	
/MuonEG/Run2016D-Nano1June2019-v1/NANOAOD	23482352 (19.4Gb)	4.2
/SingleElectron/Run2016D-Nano1June2019-v1/NANOAOD	148167727 (104.4Gb)	
/SingleMuon/Run2016D-Nano1June2019-v1/NANOAOD	98017996 (61.3Gb)	
Run 2016E		
/DoubleEG/Run2016E-Nano1June2019-v1/NANOAOD	49877710 (37.9Gb)	
/DoubleMuon/Run2016E-Nano1June2019-v1/NANOAOD	28246946 (20.8Gb)	
/MuonEG/Run2016E-Nano1June2019-v2/NANOAOD	22519303 (19.0Gb)	4.0
/SingleElectron/Run2016E-Nano1June2019-v1/NANOAOD	117321545 (86.5Gb)	
/SingleMuon/Run2016E-Nano1June2019-v1/NANOAOD	90984718 (58.7Gb)	
Run 2016F		
/DoubleEG/Run2016F-Nano1June2019-v1/NANOAOD	34577629 (26.9Gb)	
/DoubleMuon/Run2016F-Nano1June2019-v1/NANOAOD	20329921 (15.3Gb)	
/MuonEG/Run2016F-Nano1June2019-v1/NANOAOD	16002165 (13.6Gb)	3.1
/SingleElectron/Run2016F-Nano1June2019-v1/NANOAOD	70593532 (51.4Gb)	
/SingleMuon/Run2016F-Nano1June2019-v1/NANOAOD	65489554 (42.4Gb)	
Run 2016G		
/DoubleEG/Run2016G-Nano1June2019-v1/NANOAOD	78797031 (61.6Gb)	
/DoubleMuon/Run2016G-Nano1June2019-v1/NANOAOD	45235604 (34.2Gb)	
/MuonEG/Run2016G-Nano1June2019-v1/NANOAOD	33854612 (29.0Gb)	7.6
/SingleElectron/Run2016G-Nano1June2019-v1/NANOAOD	153363109 (109.2Gb)	
/SingleMuon/Run2016G-Nano1June2019-v1/NANOAOD	149912248 (94.6Gb)	
Run 2016H		
/DoubleEG/Run2016H-Nano1June2019-v1/NANOAOD	85388734 (67.7Gb)	
/DoubleMuon/Run2016H-Nano1June2019-v1/NANOAOD	48912812 (37.3Gb)	
/MuonEG/Run2016H-Nano1June2019-v1/NANOAOD	29236516 (26.0Gb)	8.6
/SingleElectron/Run2016H-Nano1June2019-v1/NANOAOD	128854598 (93.8Gb)	
/SingleMuon/Run2016H-Nano1June2019-v1/NANOAOD	174035164 (110.2Gb)	

Table A.1: Datasets collected in 2016 and considered for this analysis.

Dataset	Events (size)	\mathcal{L} [fb $^{-1}$]
Run 2017B		
/DoubleEG/Run2017B-Nano1June2019-v1/NANOAOD	58088760 (46.6Gb)	4.8
/DoubleMuon/Run2017B-Nano1June2019-v1/NANOAOD	14501767 (10.8Gb)	
/SingleElectron/Run2017B-Nano1June2019-v1/NANOAOD	60537490 (42.2Gb)	
/SingleMuon/Run2017B-Nano1June2019-v1/NANOAOD	136300266 (86.2Gb)	
/MuonEG/Run2017B-Nano1June2019-v1/NANOAOD	4453465 (4.1Gb)	
Run 2017C		
/DoubleEG/Run2017C-Nano1June2019-v1/NANOAOD	65181125 (53.8Gb)	9.7
/DoubleMuon/Run2017C-Nano1June2019-v1/NANOAOD	49636525 (39.5Gb)	
/SingleElectron/Run2017C-Nano1June2019-v1/NANOAOD	136637888 (102.5Gb)	
/SingleMuon/Run2017C-Nano1June2019-v1/NANOAOD	165652756 (109.5Gb)	
/MuonEG/Run2017C-Nano1June2019-v1/NANOAOD	15595214 (15.0Gb)	
Run 2017D		
/DoubleEG/Run2017D-Nano1June2019-v1/NANOAOD	25911432 (21.6Gb)	4.2
/DoubleMuon/Run2017D-Nano1June2019-v1/NANOAOD	23075733 (18.6Gb)	
/SingleElectron/Run2017D-Nano1June2019-v1/NANOAOD	51526710 (38.5Gb)	
/SingleMuon/Run2017D-Nano1June2019-v1/NANOAOD	70361660 (47.2Gb)	
/MuonEG/Run2017D-Nano1June2019-v1/NANOAOD	9164365 (8.9Gb)	
Run 2017E		
/DoubleEG/Run2017E-Nano1June2019-v1/NANOAOD	56233597 (49.8Gb)	9.3
/DoubleMuon/Run2017E-Nano1June2019-v1/NANOAOD	51589091 (44.4Gb)	
/SingleElectron/Run2017E-Nano1June2019-v1/NANOAOD	102121689 (81.3Gb)	
/SingleMuon/Run2017E-Nano1June2019-v1/NANOAOD	154630534 (111.0Gb)	
/MuonEG/Run2017E-Nano1June2019-v1/NANOAOD	19043421 (19.2Gb)	
Run 2017F		
/DoubleEG/Run2017F-Nano1June2019-v1/NANOAOD	74307066 (67.1Gb)	13.5
/DoubleMuon/Run2017F-Nano1June2019-v1/NANOAOD	79756560 (68.0Gb)	
/SingleElectron/Run2017F-Nano1June2019-v1/NANOAOD	128467223 (105.2Gb)	
/SingleMuon/Run2017F-Nano1June2019-v1/NANOAOD	242135500 (178.3Gb)	
/MuonEG/Run2017F-Nano1June2019-v1/NANOAOD	25776363 (26.3Gb)	

Table A.2: Datasets collected in 2017 and considered for this analysis.

Dataset	Events (size)	$\mathcal{L} [\text{fb}^{-1}]$
Run 2018A		
/DoubleMuon/Run2018A-Nano25Oct2019-v1/NANO AOD	75499908 (62.6Gb)	
/EGamma/Run2018A-Nano25Oct2019-v1/NANO AOD	327843843 (261.8Gb)	13.5
/SingleMuon/Run2018A-Nano25Oct2019-v1/NANO AOD	241608232 (167.7Gb)	
/MuonEG/Run2018A-Nano25Oct2019-v1/NANO AOD	32958503 (32.3Gb)	
Run 2018B		
/DoubleMuon/Run2018B-Nano25Oct2019-v1/NANO AOD	35057758 (28.3Gb)	
/EGamma/Run2018B-Nano25Oct2019-v1/NANO AOD	153822427 (123.1Gb)	6.8
/SingleMuon/Run2018B-Nano25Oct2019-v1/NANO AOD	119918017 (82.3Gb)	
/MuonEG/Run2018B-Nano25Oct2019-v1/NANO AOD	16211567 (15.8Gb)	
Run 2018C		
/DoubleMuon/Run2018C-Nano25Oct2019-v1/NANO AOD	34565869 (27.6Gb)	
/EGamma/Run2018C-Nano25Oct2019-v1/NANO AOD	147827904 (119.2Gb)	6.6
/SingleMuon/Run2018C-Nano25Oct2019-v1/NANO AOD	110032072 (75.7Gb)	
/MuonEG/Run2018C-Nano25Oct2019-v1/NANO AOD	15652198 (15.3Gb)	
Run 2018D		
/DoubleMuon/Run2018D-Nano25Oct2019_ver2-v1/NANO AOD	168605834 (128.6Gb)	
/EGamma/Run2018D-Nano25Oct2019-v1/NANO AOD	751348648 (583.6Gb)	32.0
/SingleMuon/Run2018D-Nano25Oct2019-v1/NANO AOD	513867253 (344.5Gb)	
/MuonEG/Run2018D-Nano25Oct2019_ver2-v1/NANO AOD	71961587 (68.6Gb)	

Table A.3: Datasets collected in 2018 and considered for this analysis.

Process	Sample	Cross section [pb]
DY	DYJetsToLL_M-10to50_TuneCUETP8M1_13TeV-madgraphMLM-pythia8	18610.0
	DYJetsToLL_M-50_TuneCUETP8M1_13TeV-madgraphMLM-pythia8	6025.20
TTTo2L2Nu	TTTo2L2Nu_TuneCUETP8M2_ttHtranche3_13TeV-powheg-pythia8	87.310
Single top	ST_s-channel_4f_leptonDecays_13TeV-amcatnlo-pythia8_TuneCUETP8M1	3.360
	ST_t-channel_antitop_4f_inclusiveDecays_13TeV-powhegV2-madspin-pythia8_TuneCUETP8M1	26.38
	ST_t-channel_top_4f_inclusiveDecays_13TeV-powhegV2-madspin-pythia8_TuneCUETP8M1	44.33
	ST_tW_antitop_5f_inclusiveDecays_13TeV-powheg-pythia8_TuneCUETP8M1	35.60
	ST_tW_top_5f_inclusiveDecays_13TeV-powheg-pythia8_TuneCUETP8M1	35.60
WW	WWTo2L2Nu_13TeV-powheg	12.178
	WWJJToLNuLNu_EWK_noTop_13TeV-madgraph-pythia8	0.34520
	GluGluWWTo2L2Nu_MCFM_13TeV	0.5905
V γ /V γ^*	WGToLNuG_TuneCUETP8M1_13TeV-madgraphMLM-pythia8	405.271
	ZGTo2LG_TuneCUETP8M1_13TeV-amcatnloFXFX-pythia8	131.300
	WZTo3LNu_mllmin01_13TeV-powheg-pythia8	58.59
VZ	ZZTo2L2Nu_13TeV_powheg_pythia8	0.5640
	ZZTo2L2Q_13TeV_powheg_pythia8	3.22
	ZZTo4L_TuneCP5_13TeV_powheg_pythia8	1.212
	WZTo2L2Q_13TeV_amcatnloFXFX_madspin_pythia8	5.595
VVV	ZZZ_TuneCUETP8M1_13TeV-amcatnlo-pythia8	0.01398
	WZZ_TuneCUETP8M1_13TeV-amcatnlo-pythia8	0.05565
	WWZ_TuneCUETP8M1_13TeV-amcatnlo-pythia8	0.16510
	WWW_4F_TuneCUETP8M1_13TeV-amcatnlo-pythia8	0.18331
Non-Prompt	Data-driven (tight-to-loose method)	

Table A.4: Main 2016 MC simulations for the different background processes considered for this analysis and their respective cross sections.

Process	Sample	Cross section [pb]
DY	DYJetsToLL_M-10to50_TuneCP5_13TeV-madgraphMLM-pythia8	18610
	DYJetsToLL_M-50_TuneCP5_13TeV-madgraphMLM-pythia8	6189.39
TTTo2L2Nu	TTTo2L2Nu_TuneCP5_13TeV-powheg-pythia8	87.310
Single top	ST_s-channel_4f_leptonDecays_mtop1715_TuneCP5_PSweights_13TeV-amcatnlo-pythia8	3.360
	ST_t-channel_antitop_4f_inclusiveDecays_TuneCP5_13TeV-powhegV2-madspin-pythia8	26.38
	ST_t-channel_top_4f_inclusiveDecays_TuneCP5_13TeV-powhegV2-madspin-pythia8	44.33
	ST_tW_antitop_5f_inclusiveDecays_TuneCP5_13TeV-powheg-pythia8	35.60
	ST_tW_top_5f_inclusiveDecays_TuneCP5_13TeV-powheg-pythia8	35.60
WW	WWTo2L2Nu_NNPDF31_TuneCP5_PSweights_13TeV-powheg-pythia8	12.178
	WWJJToLNuLNu_EWK_noTop_TuneCP5_13TeV-madgraph-pythia8	0.34520
	GluGluToWWTo*_13TeV_MCFM701_pythia8	0.06387
V γ /V γ^*	WGToLNuG_TuneCP5_13TeV-madgraphMLM-pythia8	405.271
	ZGToLLG_01J_5f_TuneCP5_13TeV-amcatnloFXFX-pythia8	58.83
	WZTo3LNu_mllmin01_NNPDF31_TuneCP5_13TeV_powheg_pythia8	58.59
VZ	ZZTo2L2Nu_13TeV_powheg_pythia8	0.5640
	ZZTo2L2Q_13TeV_amcatnloFXFX_madspin_pythia8	3.22
	ZZTo4L_TuneCP5_13TeV_powheg_pythia8	1.212
	WZTo2L2Q_13TeV_amcatnloFXFX_madspin_pythia8	5.595
VVV	ZZZ_TuneCP5_13TeV-amcatnlo-pythia8	0.01398
	WZZ_TuneCP5_13TeV-amcatnlo-pythia8	0.05565
	WWZ_4F_TuneCP5_13TeV-amcatnlo-pythia8	0.16510
	WWW_4F_TuneCP5_13TeV-amcatnlo-pythia8	0.18331
Non-Prompt	Data-driven (tight-to-loose method)	

Table A.5: Main 2017 MC simulations for the different background processes considered for this analysis and their respective cross sections.

Process	Sample	Cross section [pb]
DY	DYJetsToLL_M-10to50_TuneCP5_13TeV-madgraphMLM-pythia8	18610.0
	DYJetsToLL_M-50_TuneCP5_13TeV-amcatnloFXFX-pythia8	6189.39
TTTo2L2Nu	TTTo2L2Nu_TuneCP5_13TeV-powheg-pythia8	87.310
Single top	ST_s-channel_4f_leptonDecays_TuneCP5_13TeV-madgraph-pythia8	3.360
	ST_t-channel_antitop_4f_InclusiveDecays_TuneCP5_13TeV-powheg-madspin-pythia8	26.38
	ST_t-channel_top_4f_InclusiveDecays_TuneCP5_13TeV-powheg-madspin-pythia8	44.33
	ST_tW_antitop_5f_inclusiveDecays_TuneCP5_13TeV-powheg-pythia8	35.60
	ST_tW_top_5f_inclusiveDecays_TuneCP5_13TeV-powheg-pythia8	35.60
WW	WWTo2L2Nu_NNPDF31_TuneCP5_13TeV-powheg-pythia8	12.178
	WWJJToLNuLNu_EWK_TuneCP5_13TeV-madgraph-pythia8	0.4286
	GluGluToWWTo*_TuneCP5_13TeV_MCFM701_pythia8	0.06387
V γ /V γ^*	WGToLNuG_TuneCP5_13TeV-madgraphMLM-pythia8	405.271
	ZGToLLG_01J_5f_TuneCP5_13TeV-amcatnloFXFX-pythia8	131.300
	WZTo3LNu_mllmin01_NNPDF31_TuneCP5_13TeV_powheg_pythia8	58.59
VZ	ZZTo2L2Nu_TuneCP5_13TeV_powheg_pythia8	0.5640
	ZZTo2L2Q_13TeV_amcatnloFXFX_madspin_pythia8	3.22
	ZZTo4L_TuneCP5_13TeV_powheg_pythia8	1.212
	WZTo2L2Q_13TeV_amcatnloFXFX_madspin_pythia8	5.595
VVV	ZZZ_TuneCP5_13TeV-amcatnlo_pythia8	0.01398
	WZZ_TuneCP5_13TeV-amcatnlo_pythia8	0.05565
	WWZ_TuneCP5_13TeV-amcatnlo_pythia8	0.16510
	WWW_4F_TuneCP5_13TeV-amcatnlo_pythia8	0.18331
Non-Prompt	Data-driven (tight-to-loose method)	

Table A.6: Main 2018 MC simulations for the different background processes considered for this analysis and their respective cross sections.

Appendix B

Neural network optimization

List of figures

1.1	Structure of a pp collision and different steps of the MC simulation used by the event generators, such as the parton shower (in green), the UE (in pink), the hadronization (in blue) and the decay of unstable particles (in red) [101].	2
1.2	Top p_T (on the left) and rapidity (on the right) distributions obtained using different MC generators [110].	3
1.3	Proton energy distribution at 3 (on the left) and 6 (on the right) GeV compared for the test beam data (in black) and two different GEANT4 versions [112].	5
1.4	Production cross section of the most common SM processes considering different center of mass energies, such as the 13 TeV of the LHC.	7
1.5	Main feynman diagrams for the production of the SM $t\bar{t}$ process.	8
1.6	Feynman diagrams for s-channel production mode of a single top quarks.	8
1.7	Feynman diagrams for t-channel (on the left) and tW (on the right) production modes of a single top quarks.	9
1.8	Feynman diagrams for the leptonic decay of the top (on the left) and antitop (on the right) quarks.	9
1.9	Feynman diagram for the DY process involving a virtual γ^* or Z boson.	9
1.10	Possible Feynman diagrams for the Initial State Radiation (ISR) $t\bar{t}$ with a W/Z boson (on the left) and for the production of an Final State Radiation (FSR) ttZ (on the center and right).	10
1.11	Possible Feynman diagrams for the production of a W/Z boson with a jet.	10
1.12	Schematic representation of the two jets used for the systematics and for the jet faking a lepton in the tight-to-loose datadriven method.	11
1.13	Electron (on the left) and muon (on the right) FR obtained in a QCD enriched region for different jet E_T thresholds for 2016, 2017 and 2018 with respect to the p_T of the lepton.	13
1.14	Electron (on the left) and muon (on the right) PR obtained in a Z+jets enriched region by a general tag and probe method for 2016, 2017 and 2018 with respect to the p_T of the lepton.	14
1.15	Possible Feynman diagrams for smaller backgrounds of this analysis: WW (on the left), $W\gamma$ and WZ (on the center) and ZZ (on the right).	15

1.16 Data/MC agreement with (on the right) and without (on the left) prefireing corrections in a 2017 top control region.	16
2.1 DougleEG trigger efficiencies with respect to the p_T (on the left) and η (on the right), computed using a tag and probe method, for the 2017 data taking period.	19
2.2 Tight electron efficiencies for this analysis, based on the Egamma POG $mva_90p_Iso2016$ WP, for the data taking period of 2016.	22
2.3 Tight muon efficiencies for this analysis, based on the Muon POG tight WP with additional cuts for 2016, 2017 and 2018.	23
2.4 Same sign control region m_{ll} distributions for the years 2016, 2017 and 2018 and for the $e\mu$ channel and for the 0-jet (on the left) and 1j (on the right) categories.	26

List of tables

2.1	2016 trigger paths considered for this analysis.	18
2.2	2017 trigger paths considered for this analysis.	18
2.3	2018 trigger paths considered for this analysis.	19
2.4	Quality cuts applied to define a 2016 tight electron in this analysis.	21
2.5	Quality cuts applied to define a 2017/2018 tight electron in this analysis.	22
2.6	JET/MET POG tight WP for 2016.	24
2.7	JET/MET POG tight WP for 2017 and 2018.	24
2.8	JET/MET POG tight WP for 2017 and 2018, for jets having a $p_T > 50$ GeV.	24
A.1	Datasets collected in 2016 and considered for this analysis.	36
A.2	Datasets collected in 2017 and considered for this analysis.	37
A.3	Datasets collected in 2018 and considered for this analysis.	38
A.4	Main 2016 MC simulations for the different background processes considered for this analysis and their respective cross sections.	39
A.5	Main 2017 MC simulations for the different background processes considered for this analysis and their respective cross sections.	40
A.6	Main 2018 MC simulations for the different background processes considered for this analysis and their respective cross sections.	41

Bibliography

- [1] F. Englert and R. Brout, "Broken symmetry and the mass of gauge vector mesons", Phys. Rev. Lett. 13, pp. 321-323, 1964
- [2] P. W. Higgs, "Broken symmetries and the masses of gauge bosons", Phys. Rev. Lett. 13, pp. 508-509, 1964
- [3] S. Chatrchyan et al., "Observation of a new boson at a mass of 125 GeV with the CMS experiment at the LHC", Phys. Lett. B716, pp. 30-61, 2012 [arXiv: 1207.7235]
- [4] G. Aad et al., "Observation of a new particle in the search for the Standard Model Higgs boson with the ATLAS detector at the LHC", Phys. Lett. B716, pp. 1-29, 2012 [arXiv: 1207.7214]
- [5] V.C. Rubin, W.K. Ford and N. Thonnard, "Rotational properties of 21 SC galaxies with a large range of luminosities and radii, from NGC 4605 (R=4kpc) to UGC 2885 (R=122kpc)", Astrophysical Journal 238, pp. 471-487, 1980
- [6] K.G. Begeman, A.H. Broeils and R.H. Sanders, "Extended rotation curves of spiral galaxies - Dark haloes and modified dynamics", Monthly Notices of the Royal Astronomical Society, vol. 249, issue 3, ISSN 0035-8711, 1991
- [7] A. Robertson, R. Massey and V. Eke, "What does the Bullet Cluster tell us about self-interacting dark matter?", Monthly Notices of the Royal Astronomical Society, vol. 465, issue 1, 2017 [arXiv: 1605.04307]
- [8] J.B. Mu?oz, C. Dvorkin and A. Loeb, "21-cm Fluctuations from Charged Dark Matter", Phys. Rev. Lett. 121, 121301 (2018) [arXiv: 1804.01092]
- [9] A. Natarajan, "A closer look at CMB constraints on WIMP dark matter", Phys. Rev. D85, 2012 [arXiv:1201.3939]
- [10] G. D'Ambrosio G.F. Giudice, G. Isidori and A. Strumia, "Minimal Flavour Violation: an effective field theory approach", Nucl.Phys. 645, pp 155-187, 2002 [arXiv:0207.036]
- [11] CMS Collaboration, "Search for the production of dark matter in association with top-quark pairs in the single-lepton final state in proton-proton collisions at $\sqrt{s} = 8$ TeV", JHEP, vol. 6 121, 2015
- [12] CMS Collaboration, "Search for the Production of Dark Matter in Association with Top Quark Pairs in the Di-lepton Final State in pp collisions at $\sqrt{s} = 8$ TeV", CMS-PAS-B2G-13-004, 2014
- [13] "Search for dark matter in events with heavy quarks and missing transverse momentum in pp collisions with the ATLAS detector", Eur. Phys. J. C (2015) 75:92
- [14] ATLAS Collaboration, Search for the Supersymmetric Partner of the Top Quark in the Jets+Emiss Final State at $\sqrt{s} = 13$ TeV", ATLAS-CONF-2016-077

- [15] ATLAS Collaboration, "Search for top squarks in final states with one isolated lepton, jets, and missing transverse momentum in $\sqrt{s} = 13$ TeV pp collisions with the ATLAS detector", ATLAS-CONF-2016-050, 2016
- [16] ATLAS Collaboration, "Search for direct top squark pair production and dark matter production in final states with two leptons in $\sqrt{s} = 13$ TeV pp collisions using 13.3 fb^{-1} of ATLAS data", ATLAS-CONF-2016-076, 2016
- [17] ATLAS Collaboration, "Search for dark matter produced in association with bottom or top quarks in $\sqrt{s} = 13$ TeV pp collisions with the ATLAS detector", Eur. Phys. J. C 78 (2018) 18 [arXiv: 1710.11412]
- [18] CMS Collaboration, Search for dark matter produced in association with heavy-flavor quark pairs in proton-proton collisions at $\sqrt{s} = 13$ TeV", Eur. Phys. J. C (2017) 77: 845
- [19] CMS Collaboration, "Search for dark matter particles produced in association with a top quark pair at $\sqrt{s} = 13$ TeV", Phys. Rev. Lett. 122, 011803 (2019) [arXiv: 1807.06522]
- [20] CMS Collaboration, "Search for dark matter produced in association with a single top quark or a top quark pair in proton-proton collisions at $\sqrt{s} = 13$ TeV", JHEP, vol. 03 141, 2019 [arXiv: 1901.01553]
- [21] S. Manzoni, "The Standard Model and the Higgs Boson", Physics with Photons Using the ATLAS Run 2 Data, Springer Theses, 2019
- [22] A.B. Balantekin, A. Gouvea and B.Kayser, "Addressing the Majorana vs. Dirac Question with Neutrino Decays", FERMILAB-PUB-18-418-T, NUHEP-TH/18-09 [arXiv: 1808.10518]
- [23] J. Woithe, G.J. Wiener and F. Van der Vecken, "Let's have a coffee with the Standard Model of particle physics!", Physics education 52, number 3, 2017
- [24] F. Zwicky, "Die Rotverschiebung von extragalaktischen Nebeln", Helvetica Physica Acta , vol. 6, pp. 110-127, 1933
- [25] S. Van den Bergh, Phys Rev D "The early history of dark matter", Dominion Astrophysical Observatory, 1999
- [26] V.C. Rubin, W.K. Ford, "Rotation of the Andromeda Nebula from a Spectroscopic Survey of Emission Regions", Astrophysical Journal 159, p. 379, 1970
- [27] A. A. Penzias, R.W. Wilson, "A Measurement of Excess Antenna Temperature at 4080 Mc/s", Astrophysical Journal 142, pp. 419-421
- [28] D.J. Fixsen, "The temperature of the cosmic microwave background", Astrophysical Journal, 2009
- [29] Planck Collaboration, "Planck 2018 results. I. Overview and the cosmological legacy of Planck", 2018 [arXiv: 1807.06205]
- [30] R. Tojeiro, "Understanding the Cosmic Microwave Background Temperature Power Spectrum", 2006
- [31] Planck Collaboration, "Planck 2018 results. VI. Cosmological parameters", 2018 [arXiv: 1807.06209]
- [32] "Astrophysical Constants and Parameters", 2019
- [33] D. Clowe et all., "A Direct Empirical Proof of the Existence of Dark Matter", Astrophysical Journal Letters 648, 2006

- [34] K.R. Dienes, J. Fennick, J. Kumar, B. Thomas "Dynamical Dark Matter from Thermal Freeze-Out", Phys. Rev. D 97, 063522 (2018) [arXiv: 1712.09919]
- [35] C.S. Frenk, S.D.M. White, "Dark matter and cosmic structure", Annalen der Physik, p. 22 , 2012 [arXiv: 1210.0544]
- [36] R. Kirk, "Dark matter genesis"
- [37] M. Drewes et all., "A White Paper on keV Sterile Neutrino Dark Matter", 2016 [arXiv: 1602.04816]
- [38] C. Alcock et all., "The MACHO Project: Microlensing Results from 5.7 Years of LMC Observations", Astrophys.J. 542 (2000) 281-307
- [39] P. Tisserand et all., "Limits on the Macho content of the Galactic Halo from the EROS-2 Survey of the Magellanic Clouds", A & A 469, pp. 387-404 (2007)
- [40] EROS and MACHO collaborations, "EROS and MACHO Combined Limits on Planetary Mass Dark Matter in the Galactic Halo", 1998
- [41] Particle Data Group, "Neutrino Cross Section Measurements", PDG 2019
- [42] K. McFarland, "Neutrino Interactions", 2008 [arXiv: 0804.3899]
- [43] E. Morgan, "Aspects of WIMP Dark Matter Searches at Colliders and Other Probes", Springer theses, 2016
- [44] F. Couchot et all., "Cosmological constraints on the neutrino mass including systematic uncertainties", A & A 606, A104 (2017)
- [45] E. Bulbul et all., "Detection of An Unidentified Emission Line in the Stacked X-ray spectrum of Galaxy Clusters", 2014 [arXiv: 1402.2301]
- [46] A. Boyarsky et all., "An unidentified line in X-ray spectra of the Andromeda galaxy and Perseus galaxy cluster", Phys. Rev. Lett. 113, 251301 (2014) [arXiv: 1402.4119]
- [47] A. Boyarsky et all., "Checking the dark matter origin of 3.53 keV line with the Milky Way center", Phys. Rev. Lett. 115, 161301 (2015) [arXiv: 1408.2503]
- [48] T. Jeltema1 and S.Profumo, "Deep XMM Observations of Draco rule out at the 99% Confidence Level a Dark Matter Decay Origin for the 3.5 keV Line", 2015 [arXiv: 1512.01239]
- [49] D. Wu, "A Brief Introduction to the Strong CP Problem", Superconducting Super Collider Laboratory, 1991
- [50] R.D. Peccei, H.R. Quinn, "CP Conservation in the Presence of Pseudoparticles", Phys. Rev. Lett. 38, 1440, 1977
- [51] P.W. Graham et all., "Experimental Searches for the Axion and Axion-like Particles", Annual Review if Nuclear and Particle Science 65, 2015 [arXiv: 1602.00039]
- [52] CAST collaboration, "New CAST limit on the axion-photon interaction", Nature Physics 13, pp. 584-590 (2017)
- [53] B. Penning, "The Pursuit of Dark Matter at Colliders - An Overview", 2017 [arXiv: 1712.01391]

- [54] M. Schumann, "Direct Detection of WIMP Dark Matter: Concepts and Status", J. Phys. G46 (2019) no.10, 103003 [arXiv: 1903.03026]
- [55] S.C. Martin et all., "The RAVE survey: constraining the local Galactic escape speed", Mon.Not.Roy.Astron.Soc.379:755-772, 2007
- [56] K. Freese, M. Lisanti, C. Savage, "Annual Modulation of Dark Matter: A Review", [arXiv: 1209.3339v3]
- [57] T.M. Undagoitia and L. Rauch, "Dark matter direct-detection experiments", J. Phys. G43 (2016) no.1, 013001 [arXiv: 1509.08767]
- [58] R. Bernabei et all., "First results from DAMA/LIBRA and the combined results with DAMA/NaI", Eur.Phys.J.C56:333-355, 2008 [arXiv: 0804.2741]
- [59] J.M. Gaskins, "A review of indirect searches for particle dark matter", Contemporary Physics, 2016 [arXiv: 1604.00014]
- [60] F.S. Queiroz, "Dark Matter Overview: Collider, Direct and Indirect Detection Searches", Max-Planck Institute of Physics
- [61] LAT collaboration, "Constraints on Dark Matter Annihilation in Clusters of Galaxies with the Fermi Large Area Telescope", JCAP 05(2010)025 [arXiv: 1002.2239]
- [62] A.A. Moiseev et all., "Dark Matter Search Perspectives with GAMMA-400", 2013 [arXiv: 1307.2345]
- [63] L. Covi et all., "Neutrino Signals from Dark Matter Decay", JCAP 1004:017, 2010 [arXiv: 0912.3521]
- [64] B. Lu and H. Zong, "Limits on the Dark Matter from AMS-02 antiproton and positron fraction data", Phys. Rev. D 93, 103517 (2016) [arXiv: 1510.04032]
- [65] J. Abdallah et all., "Simplified Models for Dark Matter Searches at the LHC", Phys. Dark Univ. 9-10 (2015) 8-23 [arXiv: 1506.03116]
- [66] H. An, L. Wang, H. Zhang, "Dark matter with t-channel mediator: a simple step beyond contact interaction", Phys. Rev. D 89, 115014 (2014) [arXiv: 1308.0592]
- [67] ATLAS Collaboration, "Search for dark matter and other new phenomena in events with an energetic jet and large missing transverse momentum using the ATLAS detector", JHEP 01 (2018) 126 [arXiv: 1711.03301]
- [68] CMS Collaboration, "Search for new physics in the monophoton final state in proton-proton collisions at $\sqrt{s} = 13$ TeV", J. High Energy Phys. 10 (2017) 073 [arXiv: 1706.03794]
- [69] CMS Collaboration, "Search for dark matter produced with an energetic jet or a hadronically decaying W or Z boson at $\sqrt{s} = 13$ TeV", JHEP 07 (2017) 014 [arXiv: 1703.01651]
- [70] CMS Collaboration, "Search for new physics in final states with an energetic jet or a hadronically decaying W or Z boson and transverse momentum imbalance at $\sqrt{s} = 13$ TeV", Phys. Rev. D 97, 092005 (2018) [arXiv: 1712.02345]
- [71] ATLAS Collaboration, "Search for dark matter in association with a Higgs boson decaying to two photons at $\sqrt{s} = 13$ TeV with the ATLAS detector", Phys. Rev. D 96 (2017) 112004 [arXiv: 1706.03948]
- [72] CMS Collaboration, "Search for associated production of dark matter with a Higgs boson decaying to $b\bar{b}$ or $\gamma\gamma$ at $\sqrt{s} = 13$ TeV", JHEP 10 (2017) 180 [arXiv: 1703.05236]

- [73] Atlas Collaboration, "Search for new phenomena in dijet events using 37 fb^{-1} of pp collision data collected at $\sqrt{s} = 13 \text{ TeV}$ with the ATLAS detector", Phys. Rev. D 96, 052004 (2017) [arXiv: 1703.09127]
- [74] CMS Collaboration, "Search for narrow and broad dijet resonances in proton-proton collisions at $\sqrt{s} = 13 \text{ TeV}$ and constraints on dark matter mediators and other new particles", JHEP 08 (2018) 130 [arXiv: 1806.00843]
- [75] C. Munoz, "Models of Supersymmetry for Dark Matter", FTUAM 17/2, IFT-UAM/CSIC-17-005, 2017 [arXiv: 1701.05259]
- [76] CMS Collaboration, "Searches for invisible decays of the Higgs boson in pp collisions at $s_{\text{sqrt}s} = 7, 8, \text{ and } 13 \text{ TeV}$ ", JHEP 02 (2017) 135 [arXiv: 1610.09218]
- [77] J. Alimena et all., "Searching for long-lived particles beyond the Standard Model at the Large Hadron Collider", 2019 [arXiv: 1903.04497]
- [78] A. Albert et all., "Recommendations of the LHC Dark Matter Working Group: Comparing LHC searches for heavy mediators of dark matter production in visible and invisible decay channels", 2017 [arXiv: 1703.05703]
- [79] M. Tanabashi et al., Particle Data Group, Phys. Rev. D98, 030001 (2018)
- [80] R. Schicker, "The ALICE detector at LHC", 2005
- [81] LHCb Collaboration, "LHCb Detector Performance", Int. J. Mod. Phys. A 30, 1530022 (2015) [arXiv: 1412.6352]
- [82] J.T. Boyd, "LHC Run-2 and Future Prospects", 2020
- [83] E. Gschwendtner, "AWAKE, A Particle-driven Plasma Wakefield Acceleration Experiment", CERN Yellow Report CERN 2016-001, pp.271-288 [arXiv: 1705.10573]
- [84] M. Thomson, "Modern Particle Physics", Cambridge University Press, 2013
- [85] G. Apollinari et all., "High Luminosity Large Hadron Collider HL-LHC", CERN Yellow Report CERN-2015-005, pp.1-19 [arXiv: 1705.08830]
- [86] CMS Collaboration, "The CMS experiment at the CERN LHC", JINST 3 (2008) S08004
- [87] CMS Collaboration, "Precision measurement of the structure of the CMS inner tracking system using nuclear interactions", JINST 13 (2018) P10034 [arXiv: 1807.03289]
- [88] M.S. Kim, "CMS reconstruction improvement for the muon tracking by the RPC chambers", 2013 JINST 8 T03001 [arXiv: 1209.2646]
- [89] CMS Collaboration, "Performance of the CMS muon detector and muon reconstruction with proton-proton collisions at $\sqrt{s} = 13 \text{ TeV}$ ", JINST 13 (2018) P06015 [arXiv: 1804.04528]
- [90] CMS Collaboration, "Particle-Flow Event Reconstruction in CMS and Performance for Jets, Taus, and MET", CMS-PAS-PFT-09-001, 2009
- [91] CMS Collaboration, "Description and performance of track and primary-vertex reconstruction with the CMS tracker", JINST 9 (2014) P10009 [arXiv: 1405.6569]
- [92] V. Knunz, "Measurement of Quarkonium Polarization to Probe QCD at the LHC", Springer theses, 2015

- [93] CMS Collaboration, "Performance of electron reconstruction and selection with the CMS detector in proton-proton collisions at $\sqrt{s} = 8$ TeV", JINST 10 (2015) P06005 [arXiv: 1502.02701]
- [94] J. Rembser, "CMS Electron and Photon Performance at 13 TeV", J. Phys. Conf. Ser. 1162 012008, 2019
- [95] P.L.S. Connor, "Review of jet reconstruction algorithms", Ryan Atkin J. Phys. Conf. Ser. 645 012008, 2015
- [96] CMS Collaboration, "Jet energy scale and resolution in the CMS experiment in pp collisions at 8 TeV", JINST 12 (2017) P02014 [arXiv: 1607.03663]
- [97] F. Beaudette, "The CMS Particle Flow Algorithm", 2014 [arXiv: 1401.8155]
- [98] CMS Collaboration, "Identification of heavy-flavour jets with the CMS detector in pp collisions at 13 TeV", JINST 13 (2018) P05011 [arXiv: 1712.07158]
- [99] CMS Collaboration, "Performance of missing transverse momentum reconstruction in proton-proton collisions at $\sqrt{s} = 13$ TeV using the CMS detector", JINST 14 (2019) P07004 [arXiv: 1903.06078]
- [100] L. Sonnenschein, "Analytical solution of ttbar dilepton equations", Phys.Rev.D73:054015, 2016
- [101] M.H. Seymour and M. Marx, "Monte Carlo Event Generators", MCnet-13-05, 2013 [arXiv:1304.6677]
- [102] B. Cabouat, J.R. Gaunt and K. Ostrolenk, "A Monte-Carlo Simulation of Double Parton Scattering", JHEP11(2019)061 [arXiv: 1906.04669]
- [103] R. Placakyte, "Parton Distribution Functions", 2011 [arXiv:1111.5452]
- [104] J. Alwall et all., "MadGraph 5 : Going Beyond", 2011 [arXiv:1106.0522]
- [105] C. Oleari, "The POWHEG-BOX", Nucl.Phys.Proc.Suppl.205-206:36-41 [arXiv:1007.3893]
- [106] S. Frixione et all., "The MC@NLO 4.0 Event Generator", CERN-TH/2010-216 [arXiv: 1010.0819]
- [107] B. Webber, "Parton shower Monte Carlo event generators", Scholarpedia
- [108] M. Bahr et all., "Herwig++ Physics and Manual", Eur.Phys.J.C58:639-707, 2008 [arXiv: 0803.0883]
- [109] T. Sjostrand, "A Brief Introduction to PYTHIA 8.1" Comput.Phys.Commun.178:852-867, 2008 [arXiv: 0710.3820]
- [110] A. Karneyeu et all., "MCPLLOTS: a particle physics resource based on volunteer computing", European Physical Journal C 74 (2014) [arXiv: 1306.3436]
- [111] V. Lefebure and S. Banerjee, "CMS Simulation Software Using Geant4", CMS-NOTE-1999-072, 1999
- [112] S. Banerjee, "Validation of Geant4 Physics Models Using Collision Data from the LHC", J. Phys.: Conf. Ser. 898 042005
- [113] A. Rizzi, G. Petrucciani and M. Peruzzi, "A further reduction in CMS event data for analysis: the NANO AOD format", J. Phys.: Conf. Ser. 214 06021

- [114] C.G. Lester and D.J. Summers, "Measuring masses of semi-invisibly decaying particles pair produced at hadron colliders", Phys.Lett.B463:99-103, 1999
- [115] K. Bloom, "CMS software and computing for LHC Run 2", ICHEP 2016 [arXiv: 1611.03215]
- [116] W. Tanenbaum, "A ROOT/IO Based Software Framework for CMS", ECONFC0303241:TUKT010, 2003
- [117] CMS Collaboration, "CMS Luminosity Measurements for the 2016 Data Taking Period", CMS-PAS-LUM-17-001, 2017
- [118] CMS Collaboration, "CMS Luminosity Measurements for the 2017 Data Taking Period", CMS-PAS-LUM-17-001, 2018
- [119] CMS Collaboration, "CMS Luminosity Measurements for the 2018 Data Taking Period", CMS-PAS-LUM-17-001, 2019
- [120] CMS Twiki, "Reweighting recipe to emulate Level 1 ECAL prefireing"
- [121] CMS Collaboration, "Measurement of the differential cross sections for top quark pair production as a function of kinematic event variables in pp collisions at $\sqrt{s} = 7$ and 8 TeV", Phys. Rev. D 94 (2016) 052006 [arXiv: 1607.00837]
- [122] CMS Twiki, "Electron and Photon Physics Object Offline Guide"
- [123] CMS Twiki, "Baseline muon selections for Run-II", 2019
- [124] CMS Twiki, "Jet Identification"
- [125] CMS Twiki, "Heavy flavor identification at CMS with deep neural networks"
- [126] CMS Collaboration, "BRIL Work Suite"